Oceanography of the Mediterranean Sea

An Introductory Guide

Edited by

Katrin Schroeder
Consiglio Nazionale delle Ricerche-Istituto di Scienze Marine (CNR-ISMAR), Venezia, Italy

Jacopo Chiggiato
Consiglio Nazionale delle Ricerche-Istituto di Scienze Marine (CNR-ISMAR), Venezia, Italy

ELSEVIER

CHAPTER

7 Dense and deep water formation processes and Mediterranean overturning circulation

Nadia Pinardi[1], Claude Estournel[2], Paola Cessi[3], Romain Escudier[4], Vladyslav Lyubartsev[5]

[1]*Alma Mater Studiorum University of Bologna, Department of Physics and Astronomy, Bologna, Italy;* [2]*CNRS, LEGOS, Toulouse, France;* [3]*Scripps Institution of Oceanography, San Diego, CA, United States;* [4]*Mercator Ocean, Toulouse, France;* [5]*Centro EuroMediterraneo sui Cambiamenti Climatici, Bologna, Italy*

Learning Objectives

In this chapter, you will learn:
- What are the characteristics of Mediterranean dense and deep waters and their formation rates
- Where and when dense water formation processes have been observed in the Mediterranean
- What are the main formation areas
- What is the difference between dense shelf water cascading and open ocean convection
- What is the theoretical framework of these processes
- How can these processes be represented by numerical models
- What is the structure of the Mediterranean overturning cells

7.1 General concepts

The first scientific investigations into dense/deep water formation (DWF) events were conducted in the Mediterranean Sea, and were inspired by the early attempts of the oceanographic community to work together on common and critical science issues related to oceanographic processes. Henry Stommel et al. (1971) wrote in his inspiring article "Submarine clouds in the Deep Ocean" that: "Boyhood readers of Jules Verne will remember [.] the great funnel-shaped vortex that sucks ships down to the bottom of the ocean. [.] Nothing like that portrayed by Verne [.] occurs in the open sea. In fact nearly everywhere there is a permanent density stratification in the ocean [.] that affects a buoyant stability against vertical displacement of volumes of water and inhibits vertical displacement of large amplitude." Thus, the scientific

Oceanography of the Mediterranean Sea. https://doi.org/10.1016/B978-0-12-823692-5.00009-1

questions formulated were that if water buoyancy only changes at the surface, how and where does surface-transformed water reach the bottom? How is it possible to capture an event of large vertical velocities and sinking to the ocean bottom? What arrays of measurements are required, where should they be placed, and for what duration? An international group of oceanographers (MEDOC Group, 1970) from the US, UK, France and Italy conducted the first observational experiment into how DWF events occur. This took place in the offshore area of the Gulf of Lion in January to March 1969. Between February 7 and 11, this MEDOC Group (1970) gathered the first complete and undisputable evidence of water homogenization from the surface to a depth of 1000 m. The original data were published 1 year after the experiment and are shown in Fig. 7.1, showing a water column that is completely homogeneous in terms of temperature and salinity down to approximately 1500 m, which was not observed during the January investigations (not shown, see Anati and Stommel (1970) for more details). The Mediterranean remains an important area for investigations about water mass transformations.

The World Ocean Database 2018 (WOD18, Boyer et al., 2018) retains the stations from this initial experiment, although they have been redrawn with modern computer mapping algorithms and displayed similarly to those in Fig. 7.2. The station metadata are given in Table 7.1 and, although there are some omissions, the emerging picture is similar to the original. A lens of high-salinity water at the bottom

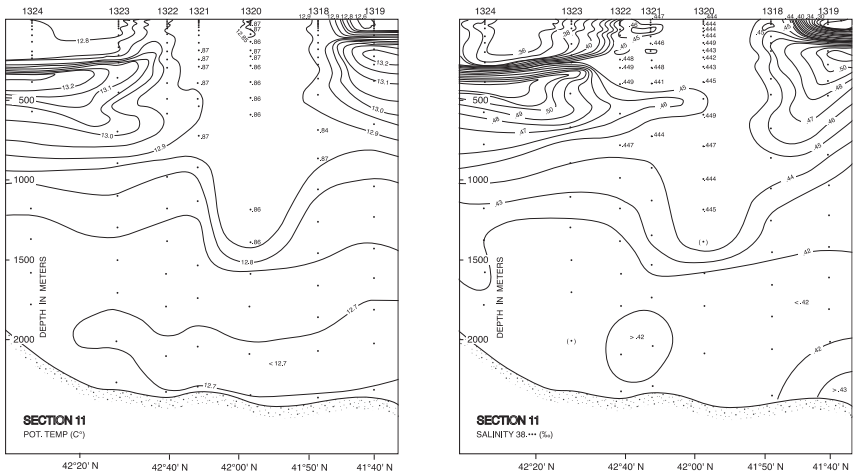

FIGURE 7.1

The stations are indicated by the numbers at the top. Data were collected between February 7–11, 1969 by the RV Atlantis II. Left panel: the potential temperature is shown in $^\circ C$°C and, in the region of the mixed patch, as any departure from 12°C of 2 decimal digits. Right panel: the salinity is shown as the departure from the reference value of 38 of 2 significant digits and with 3 in the mixed patch.

Reproduced from MEDOC Group, 1970. Observation of formation of deep water in the Mediterranean Sea, 1969. Nature, 227.

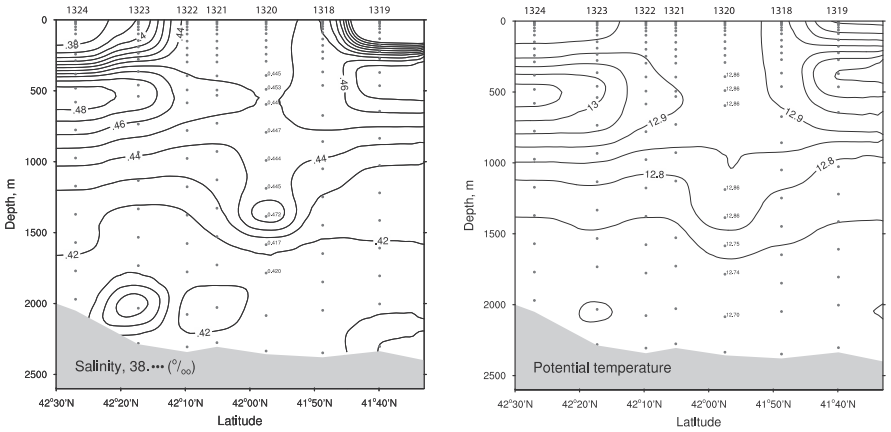

FIGURE 7.2

The objectively mapped stations corresponding to the original section represented in Fig. 7.1. Station data were retrieved from the WOD18 database and are described in Table 7.1.

of the unstratified dense water patch is now evident, which was not present in the original section. This highlights the interplay between stratification conditions, buoyancy losses, and homogenization of the water column in the process of open ocean DWF.

In the following sections, an overview of the dense/deep water characteristics and the formation rates in the Mediterranean Sea is given, with a focus on areas where dense/deep waters are formed and providing evidence for their interannual variability. In addition, the observations over the past 40 years that have followed the MEDOC's experiment are summarized. The theory of open ocean convection and shelf dense water cascading is then described, along with realistic numerical modeling of the water mass formation processes. Finally, the vertical circulation structure of the Mediterranean Sea is discussed.

7.2 Dense/deep water characteristics and formation rates

The antiestuarine character of the Mediterranean Sea is due to the specific buoyancy and momentum fluxes at the air-sea interface and determines the transformation of the entering Atlantic water (AW) into intermediate, dense and deep Mediterranean Waters (MW). These intense, diabatic, and spatially widespread water transformations occur in both the open ocean and on the shelf. The cascading of the dense waters from the shelf contributes to the intermediate water volume and to DWF in several regions of the Mediterranean.

The basic mechanism of DWF in the upper water column is through water transformation processes due to buoyancy exchanges. These dense waters can ventilate

Table 7.1 The MEDOC stations metadata shown in Fig. 7.1 by the MEDOC Group (1970) and in 8.2 with modern visualization methods.

Transect station	MEDOC station ID	WOD cast ID	Date	Time	Longitude	Latitude	Bottom depth, m
1	1324	560959	1969.02.11	00:00	5.15	42.45	2050
2	1323	6694504	1969.02.10	00:00	5.355	42.288	2287
3	1322	6694505	1969.02.10	00:00	5.363	42.162	2342
4	1321	6694500	1969.02.10	00:00	5.398	42.085	2305
5	1320	6694501	1969.02.10	00:00	5.45	41.958	2357
6	1318	6694415	1969.02.07	13:06	5.38	41.812	2329
7	1319	560605	1969.02.08	00:02	5.38	41.665	2336

the intermediate depths or become deep waters, depending on the specific mixing and spreading mechanisms, which are discussed later. Here the "source" regions of various dense water types throughout the Mediterranean Sea are examined.

The dense water masses of the Mediterranean have been classified by several authors, and an overview is given in Table 7.2. Their formation areas are located in nine regions, as indicated by the boxes in Fig. 7.3. All of the DWF areas are located in the northern part of the basin, where buoyancy fluxes may reach critical values, break the basin stratification and convect waters to the bottom. The red boxes indicate the shelf DWF areas, while the blue boxes indicate the open ocean convection areas, for both intermediate and deep waters. The shelf dense waters are characterized by cooled and well mixed waters, which then cascade into the open ocean areas at various depths. The shelf dense waters can directly affect the DWF processes, as described in Sections 7.4 and 7.5. In the areas where deep waters are formed by open ocean convection processes, the water may be convected down to the bottom, reaching $>$1200 m in the Adriatic and $>$2000$-$3000 m in the Rhodes Gyre area, Cretan Sea, and Gulf of Lion area. Such deep waters directly renew the abyssal waters of the formation area. Note that the literature sometimes refers to Eastern Mediterranean Deep Water (EMDW), which is not present in the table. This generic term is applied to deep waters in the Eastern Mediterranean Sea (EMED) that can originate from the AdDW, the CDW, the LDW, or combinations of these.

First the different estimation methods for the water mass formation rates are described, as well as the associated vertical circulation. Methods that estimate the volume formed per unit of time include that firstly described by Speer and Tziperman (1992), which computes the water mass formation rate from surface buoyancy fluxes. These give an upper limit for water transformed from light surface to denser intermediate and deep waters. This method is effective if the atmospheric conditions and surface densities are known. Second, the method described by Lascaratos (1993) estimates the formation rate from the maximum volume of the water mass in the mixed layer, which is then divided by one year. Recent papers such as those of Pinardi et al. (2015) and Simoncelli et al. (2018) apply this method, as reported in Fig. 7.4. Somot et al. (2018) recently evaluated the formation rate by comparing the maximum water mass volume in the whole water column within the formation area in one year with the minimum of this volume in the previous year, as illustrated in Fig. 7.5. The rates indicate that water mass formation occurs continuously over three- to five-year periods and then stops, which is a phenomenon yet to be fully understood. It may be connected to year-to-year preconditioning and other yet unidentified remote effects.

Fig. 7.6 illustrates the formation rate of the WMDW, as computed from the daily outputs of the latest Mediterranean Sea reanalysis products by all three of the methods described (Escudier et al., 2021). The estimations of the formation rate are similar, despite the different approaches. Selecting one method over another depends on the data available and their accuracy.

Table 7.2 Dense, Deep and Intermediate water mass characteristics in the Mediterranean Sea at the area of formation indicated in Fig. 7.3.

Water Mass name	Acronym	T-S range	Area of formation	Reference literature
Adriatic Deep Water	AdDW	T = 13 S = 38.6	4	Artegiani et al. (1997) Gacic et al. (2001) Mantziafou and Lascaratos (2004) Theocharis et al. (2014) Verri et al. (2018) Manca et al. (2003)
Northern Adriatic Dense Water	NAdDW	T = 9 −11.3 S = 38.3 −38.5	6	Artegiani et al. (1997) Orlić et al. (1992) Supić and Vilibić (2006) Wang et al. (2006) Marini et al. (2010) Theocharis et al. (2014)
Mid-Adriatic Dense Water	MAdDW	T = 11 −12.3 S = 38.2 −38.6	5	Cushman-Roisin et al. (2001) Artegiani et al. (1997) Marini et al. (2010)
Aegean Dense Water	AgDW	T = 10 S = 38.4	3	Gertman et al. (2006) Zervakis et al. (2000)
Cretan Deep Water	CDW	T = 14 −14.5 S = 38.9 −39.1	2	Theocharis et al. (1999) Theocharis et al. (2014) Velaoras et al. (2014) Velaoras et al. (2021)
Cretan Intermediate Water	CIW	T = 14.5 −15.5 S = 38.95 −39.1	2	Schlitzer et al. (1991) Theocharis et al. (1999)
Levantine Deep Water	LDW	T = 13.5 −14 S = 38.7 −38.8	1	Lascaratos (1993) Gertman et al. (1994)

Table 7.2 Dense, Deep and Intermediate water mass characteristics in the Mediterranean Sea at the area of formation indicated in Fig. 7.3.—*cont'd*

Water Mass name	Acronym	T-S range	Area of formation	Reference literature
				Theocharis et al. (2014)
Levantine Intermediate Water	LIW	T = 15 −16 S = 38.95 −39.05	1	Wüst (1961) Lascaratos (1993)
Tyrrhenian Intermediate Water	TIW	T = 13.2 −14 S = 38 −38.2	7	Napolitano et al. (2019)
Western Intermediate Water	WIW	T = 13 S = 37.7 −38.3	9	López-Jurado et al. (1995) Juza et al. (2019) Fuda et al. (2000)
Western Mediterranean Deep Water	WMDW	T = 12.70 S = 38.40	8	Pinardi et al. (2015) Somot et al. (2018)

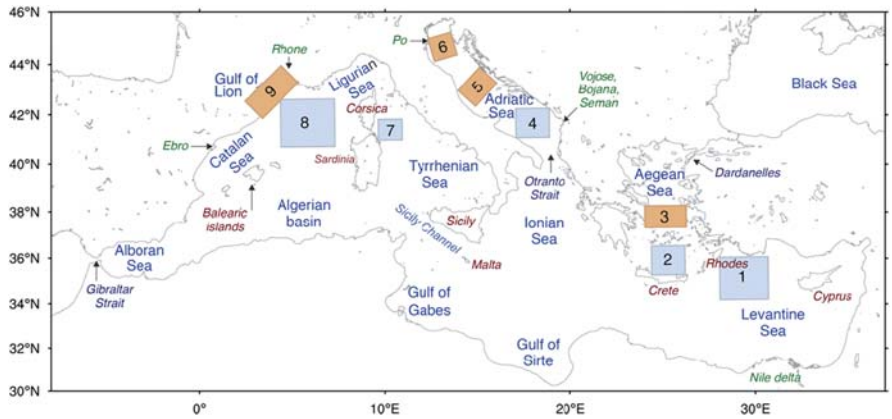

FIGURE 7.3

The nine areas where dense/deep and intermediate water formation occurs, as documented in observational and modeling studies over the past 40 years. Area 1 is the Levantine Intermediate (LIW) and Deep Water (LDW) formation area, Area 2 the Cretan Intermediate Water (CIW) and Deep Water (CDW) formation area, Area 3 the Cyclades Plateau where Aegean shelf Dense Water (AgDW) is formed, Area 4 the DWF area of the Southern Adriatic Sea (AdDW), Areas 5 and 6 are shelf DWF areas in the Middle (MAdDW) and Northern Adriatic Sea (NAdDW), respectively, Area 7 is the Tyrrhenian Intermediate Water (TIW) formation area, Area eight the Western Mediterranean Deep Water (WMDW) formation area, Area 9 is the shelf DWF area in the Gulf of Lion. Western Intermediate Water (WIW) is formed in Areas 8 and 9. Blue boxes indicate open ocean convection areas, red boxes shelf dense cascading areas.

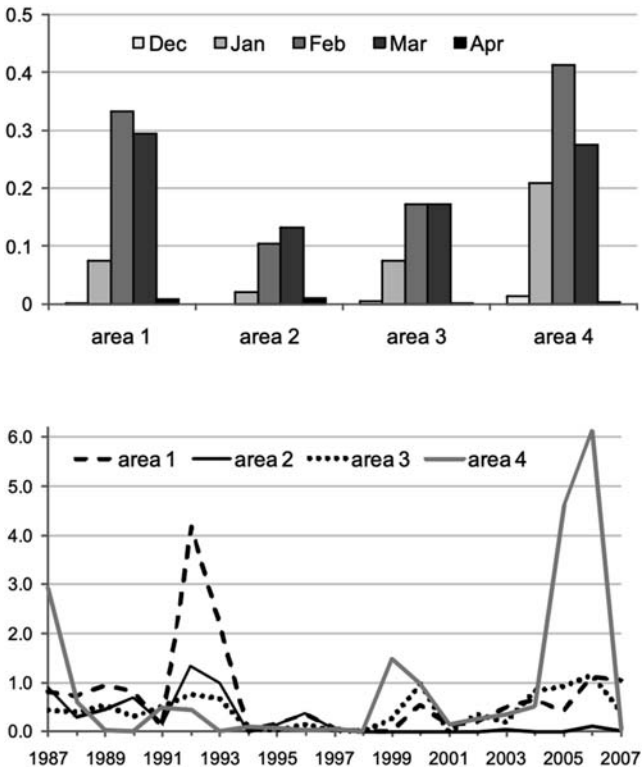

FIGURE 7.4

DWF rates in areas 1, 2, 3 and 4 of (Pinardi et al., 2015) that correspond to areas 1, 2, 4 and 8 of Fig. 7.3

Modified from Pinardi, N., Zavatarelli, M., Adani, M., Coppini, G., Fratianni, C., Oddo, P., Simoncelli, S., Tonani, M., Lyubartsev, V., Dobricic, S., Bonaduce, A., 2015. Mediterranean Sea large-scale low-frequency ocean variability and water mass formation rates from 1987 to 2007: a retrospective analysis. Prog. Oceanogr. 132, 318–332.

7.3 Observations of deep/dense water formation in the Mediterranean Sea

In the following, the DWF observations over the past 50 years in the Mediterranean Sea will be discussed. In the first part, the focus is on the Gulf of Lion because it is the most studied formation area in the region. Subsequently, observations from other dense, deep, and intermediate water formation regions of the basin will be described.

7.3.1 Convection and deep water formation in the Gulf of Lion: five decades of observations

Repeated measurements before the 1960s in the northern part of the western Mediterranean Sea (WMED) along north-south hydrographic sections revealed a permanent doming of the isopycnal surfaces associated with a cyclonic circulation.

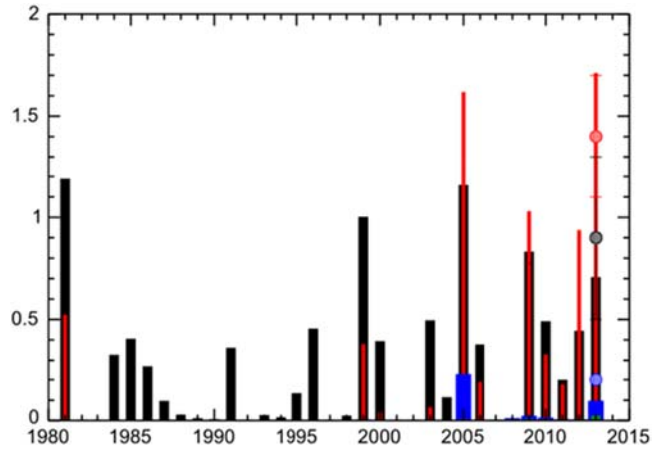

FIGURE 7.5

Interannual time series of the yearly DWF rate for WMDW area (in Sv) for the model (thick bars) and for the observation-based indicators with error bars (dotted circles Waldman et al., 2016). DWF rates using different density thresholds are shown: 29.10 kg m^{-3} (black), 29.11 kg m^{-3} (red), 29.12 kg m^{-3} (blue) and 29.13 kg m^{-3} (green).

From Somot, S., Houpert, L., Sevault, F., Testor, P., Bosse, A., Taupier-Letage, I., Bouin, M.N., Waldman, R., Cassou, C., Sanchez-Gomez, E., Durrieu de Madron, X., Adloff, F., Nabat, P., Herrmann, M., 2018. Characterizing, modelling and understanding the climate variability of the deep water formation in the North-Western Mediterranean Sea. Clim. Dynam. 51, 1179–1210.

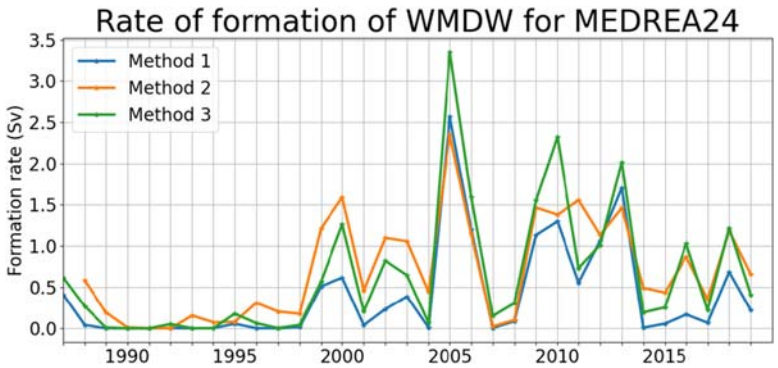

FIGURE 7.6

DWF rates for WMDW computed from the outputs of a Mediterranean Sea Reanalysis (Escudier et al., 2021) over the past 32 years. The yearly rates are estimated differently in the three methods. Method 1 is based on the air-sea fluxes (Speer and Tziperman, 1992), Method 2 uses the yearly maximum of the volume of dense water in the mixed layer (Lascaratos et al., 1993) and Method 3 the evolution of the total volume of dense water (e.g., Somot et al., 2018). For all methods, the density threshold used is 29.11 kg m^{-3}.

Tchernia (1960) noted that this doming should favor the formation of deep water. During the cold winter of 1963 (Sankey, 1973), hydrographic measurements conducted along the 6°E meridian revealed homogeneous profiles over the entire water column (0−2500 m). These measurements were repeated over the winter and a significant spatial and temporal variability was observed. At the beginning of the cold period, a station characterized by deep mixing was located less than 10 km from those where the stratification followed the classical three-layer structure of this region, consisting of AW, LIW and WMDW (see Table 7.2 for water mass names). After a month of severe cold weather, the vertically homogenized zone extended over a much wider area and occupied portions of the explored section for as far as 75 km. However, during the following much milder winter, no rupture of the three-layer structure was observed. These pioneering observations indicated the geographical area occupied by convection and also revealed that a dense network of measurements was necessary to accurately describe such a rapid oceanic process in space and time. The international measurement campaign MEDOC69 was thus conducted in 1969, using six oceanographic vessels (MEDOC Group, 1970) and samples were taken in the Gulf of Lion and the Ligurian Sea over 3 months.

The observations obtained through MEDOC69 have led to major advances in the general understanding of the processes associated with DWF, and the specific processes in the northern WMED formation area. First, this region is exposed to the Mistral in the Rhone valley and the Tramontane between the Massif Central and the Pyrenees, the dominant northerly winds that are channeled and intensified by the continental orography. In winter, these winds can be associated with cold and dry (<5°C) polar air masses blowing over the sea surface, which can be as cold as 13°C. The sea surface undergoes strong cooling through evaporation, which increases its water density. This results in an unstable vertical stratification that produces convective mixing between the surface layer and the underlying layers. Low stratification of the deep waters characterizes the northern WMED, and thus the erosion of the stratification of surface and intermediate waters by winter storms represents the critical point for deep convection (Anati and Stommel, 1970).

The extreme homogeneity of the temperature profile measured at some stations in 1969 (Fig. 7.1) reflected the intensity of the vertical mixing. In the horizontal direction, the mixing affected an area of about 50 km in the north-south direction and 130 km in the west-east direction. Unlike the vertical direction, the properties of the mixed water mass were not homogeneous horizontally within this patch of dense water (or "chimney"), because of the nonuniform thickness of the mixing. Current measurements were also conducted, which revealed increasing velocities at the cessation of the wind, with typical values of 15−20 cm s^{-1} at the surface. The horizontal structure of the current was not discerned as the number of measurements was limited, although a series of measurements carried out three weeks after the cessation of the wind showed the presence of at least three eddies of about 20 km in diameter (Sankey, 1973). Neutrally buoyant floats equipped with inclined vanes so they rotated in a vertical current were used to measure the vertical velocity (Stommel et al., 1971), and measured intensities of up to 2.5 cm s^{-1}.

The understanding of the development of open ocean convection and the processes at work increased significantly after these early observations, but some questions remained unanswered. The vertical structure of the currents, the horizontal structure of the dense water patch and the quantity of water formed were not fully understood. In the 1980 and 1990s, new observations provided further insights into the structure of currents. First, Millot (1987) identified hourly averaged current bursts near the bottom of up to 0.5 m s^{-1} during winter storms (compared to summer near-bottom currents of the order of 0.03 m s^{-1}). Further advances in current measurements were achieved through the second MEDOC experiment, the so-called MEDOC87 (Leaman and Schott, 1991; Schott and Leaman, 1991). In this experiment, Acoustic Doppler Current Profilers (ADCP) were positioned on three moorings within the center of the convection zone. These observations confirmed the presence of vertical shear in the horizontal currents, which were organized in a surface-cyclonic circulation. They also revealed the presence of relatively strong barotropic currents ($\sim$0.4 m s^{-1}) in the mixed patch zone. Finally, the ADCPs enabled vertical velocities to be characterized much more systematically than before. Downward velocities of 5−10 cm s^{-1} were recorded (Fig. 7.7A), separated by lower upward velocities (Schott and Leaman, 1991). Schott et al. (1994) used ADCP data from a new experiment in 1992 (the THETIS experiment), and found that the diameter of these cells or plumes was around 300−500 m.

Schott and Leaman (1991) summarized these observations and proposed classifying the horizontal scales during convection into three regimes: first, the scale of an homogeneous dense water patch or chimney enclosing the convection zone, which is typically of the order of 100 km; second, the scale of eddies detached from the front, which are of the order of the Rossby deformation radius (5 km); and third, the scale of convective plumes of less than 1 km.

In 2012−13, a series of campaigns was conducted using glider paths through the convection zone (Estournel et al., 2016a; Testor et al., 2018). These autonomous platforms have provided extensive information about small-scale vertical velocity structures in the dense water patch (Fig. 7.7B). Margirier et al. (2017) provided a 3D description of these plumes and a statistical description of their distribution. They have typical vertical velocities of 10−20 cm s^{-1}, a mean radius of 350 m, and are spaced apart about 2 km, covering about 30% of the convection area. The upward velocities are three times lower than the downward velocities and cover the remainder of the area. The glider observations also revealed the presence of different types of Submesoscale Coherent Vortices (SCV, McWilliams, 1985). Some of these SCV are cyclonic and others anticyclonic eddies of 5−8 km in radius and are composed of newly formed water expelled from the convection patch. Their vertical extension can reach that of the entire water column for cyclones (Bosse et al., 2016). These SCV can survive until the following winter and disperse dense water while preserving its characteristics (temperature and salinity). SCV can also encourage local convection the following winter.

The convection zone is illustrated in detail in Fig. 7.8. A complex pattern of currents develop at the edge of the zone, in the form of alternating patterns of downward/

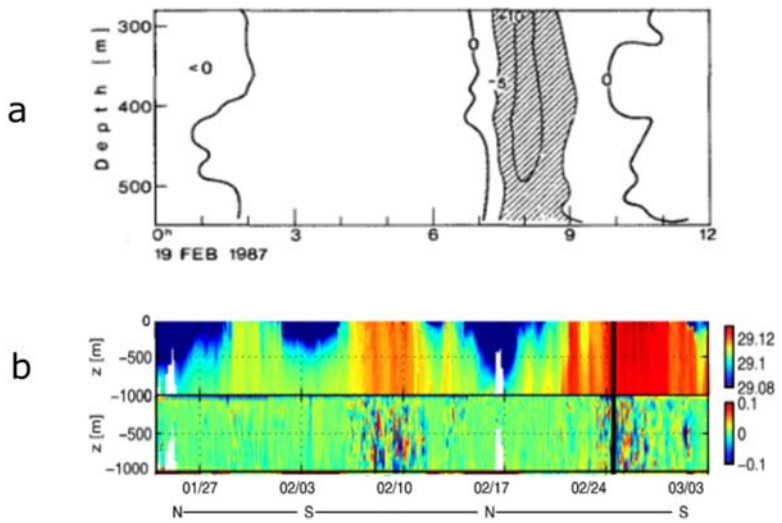

FIGURE 7.7

Characterization of vertical velocity during convective events in the Gulf of Lion with two experiments, 25 years apart. (A) ADCP observations (cm s^{-1}) in February 1987, with the horizontal axis indicating a distance (km) along a measurement section. (B) North-south glider transects in February 2013, where (top panel) shows potential density anomaly (σ_θ, kg m^{-3}) and (bottom panel) shows vertical velocity (m s^{-1}), with the horizontal axis indicating time (mm/dd). Vertical velocities associated with the dense and well-mixed water column correspond to two convective episodes of approximately 3 days following buoyancy losses, on 8–11 and 24–27 February 2013. N and S represent the northern and southern limits of the glider transects.

(A) From Schott, F., Leaman, K.D., 1991. Observations with moored acoustic Doppler current profilers in the convection regime in the Golfe du Lion. J. Phys. Oceanogr. 21 (4), 558–574, © American Meteorological Society, used with permission. (B) From Margirier, F., Bosse, A., Testor, P., L'Heveder, B., Mortier, L., Smeed, D., 2017. Characterization of convective plumes associated with oceanic deep convection in the northwestern Mediterranean from high-resolution in situ data collected by gliders. J. Geophys. Res. Oceans 122, 9814–9826.

outward cold water and upward/inward warm water. Bosse et al. (2021) proposed that symmetric instability is a major vertical and horizontal mixing process that particularly develops along fronts where wind and currents flow in the same direction.

Schroeder et al. (2010) analyzed the anomalous WMDW formation in 2004 and 2005 winter periods and deduced from observations that the contributions of atmospheric forcing and LIW lateral advection were equally important in setting the new deep water properties. Margirier et al. (2020) also documented an interplay between LIW warming and salting trends and the occurrence of deep ocean convection in the Gulf of Lion. Annual open ocean DWF events characterized the period between

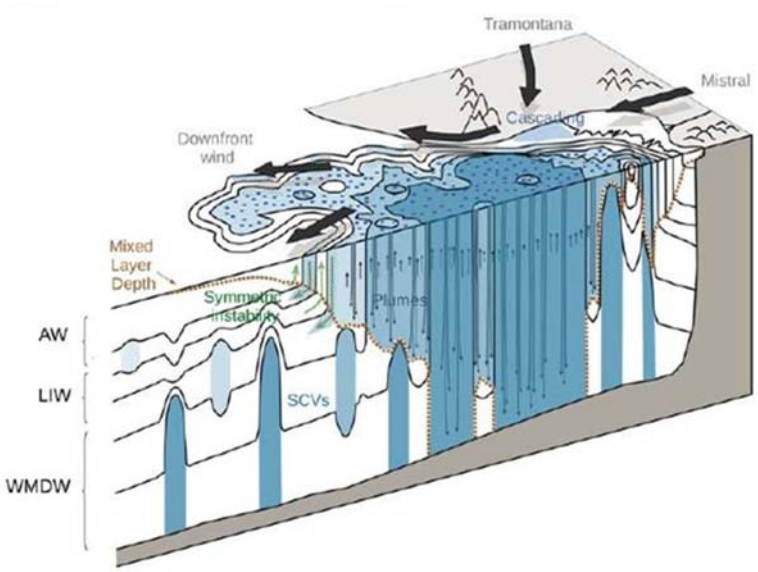

FIGURE 7.8

Scheme of the different processes at work during a major convection event in the Gulf of Lion in 2013: the inside of the dense water patch with narrow downward plumes and larger upward motions, submesoscale coherent cyclonic vortices that locally favor and/or disperse dense water, and symmetric instability along the downwind fronts.

From Testor, P., Bosse, A., Houpert, L., Margirier, F., Mortier, L., Legoff, H., Dausse, D., Labaste, M., Karstensen, J., Hayes, D., Olita, A., Ribotti, A., Schroeder, K., Chiggiato, J., Onken, R., Heslop, E., Mourre, B., D'ortenzio, F., Mayot, N., Lavigne, H., de Fommervault, O., Coppola, L., Prieur, L., Taillandier, V., Durrieu de Madron, X., Bourrin, F., Many, G., Damien, P., Estournel, C., Marsaleix, P., Taupier-Letage, I., Raimbault, P., Waldman, R., Bouin, M.N., Giordani, H., Caniaux, G., Somot, S., Ducrocq, V., Conan, P., 2018. Multiscale observations of deep convection in the northwestern Mediterranean Sea during winter 2012–2013 using multiple platforms. J. Geophys. Res. Oceans 123, 1745– 1776.

2009 and 2013, in which the LIW properties were transferred to the deep layers. During the following years (2014−18), the lack of convection produced a warming and salinification of the intermediate layers in the convection zone and the deep waters restratified making it increasingly difficult for convection to develop.

7.3.2 Deep water formation in the eastern Mediterranean

7.3.2.1 The Adriatic Sea as a main contributor to Eastern Mediterranean deep waters

The Adriatic Sea was previously identified as the largest source of the bottom water of the EMED (Pollak, 1951; Wüst, 1961; Schlitzer et al., 1991). The South Adriatic pit reaches a depth of 1200 m, is connected to the EMED through the Strait of Otranto at a depth of 800 m, and is a typical open sea DWF site. Fewer studies of

the physical processes in the Adriatic have been conducted than in the Gulf of Lion, but numerous observations reveal the interactions between the different water masses and enable us to evaluate the quantities of water formed and the dispersal pathways to the EMED.

Manca et al. (2003) analyzed hydrographic and current measurements taken during the period from March 1997 to March 1999 in the Southern Adriatic and in the Otranto Strait. During winter, the Adriatic is subject to violent north-easterly dry winds (Bora) that produce intense heat loss. Convective mixing involves surface waters and intermediate waters entering from the Otranto Strait as part of the cyclonic circulation of the Adriatic Sea. Mixing down to 800 m was observed during the winter of 1999, with a density in the range of about 29.16−29.17 kg m^{-3} (Manca et al., 2003). Below this layer of locally formed AdDW (Table 7.2), a denser water layer reached 29.34 kg m^{-3}, corresponding to NadDW (Table 7.2). A mixture of the newly formed AdDW and NAdDW exits the Adriatic through the Otranto Strait as a 200 m thick vein at a maximum velocity of 12 cm s^{-1} down-sloping in the Ionian Sea as a deep western boundary current and plunging to the bottom of the EMED (Robinson et al., 1992). Roether and Schlitzer (1991) found a mean formation rate of AdDW of 0.3 Sv using tracers. Over 3 years, the dense water outflow rate was estimated to vary from about 0.1 to 0.4 Sv (Manca et al., 2003).

The southern Adriatic appears to have much more variable water mass characteristics than the Gulf of Lion, which reflects the specific combination of lateral advective and surface buoyancy forcings, producing an open ocean convection of weaker intensity. Malanotte-Rizzoli and Robinson (1994) and Kokkini et al. (2020) investigated the impact of the Ionian circulation on the salinity of surface and intermediate waters in the southern Adriatic. During Ionian cyclonic periods (see also Chapter 9, Pinardi et al., 1997; Demirov and Pinardi, 2002; Vigo et al., 2005) high-salinity surface and intermediate water masses from the Levantine and Aegean areas enter the southern Adriatic, thus leading to dense water preconditioning, while an Ionian anticyclonic circulation leads to the advection of fresher AW.

As will be explained more in detail in Chapter 9, Adriatic winter convection produces saltier and warmer or fresher and colder dense waters, depending on the sign of this circulation (Bensi et al., 2013). Kokkini et al. (2020) showed that during a rainy year/season, high river discharges from the North Adriatic and from the Po can lead to a significant amount of fresher water being advected into the South Adriatic, which prevents DWF (the topography of the Gulf of Lion does not allow for rivers to have a significant impact in the convection zone). The combination of variable low-salinity water volumes from the northern Adriatic, high salinity inflow from Otranto, and variable buoyancy fluxes at the sea surface can lead to complex stratifications in the Southern Adriatic preconditions, such as the presence of a salinity double maximum in 2015 and 2016 (Fig. 7.9). Bensi et al. (2013) demonstrated that the arrival of very dense NAdDW in the South Adriatic pit could contribute to the deep waters of the EMED, with anomalous properties. In addition, the Adriatic Sea is a semienclosed basin, which distinguishes it from the open ocean DWF processes of the Gulf of Lion, and thus creates specific conditions for DWF.

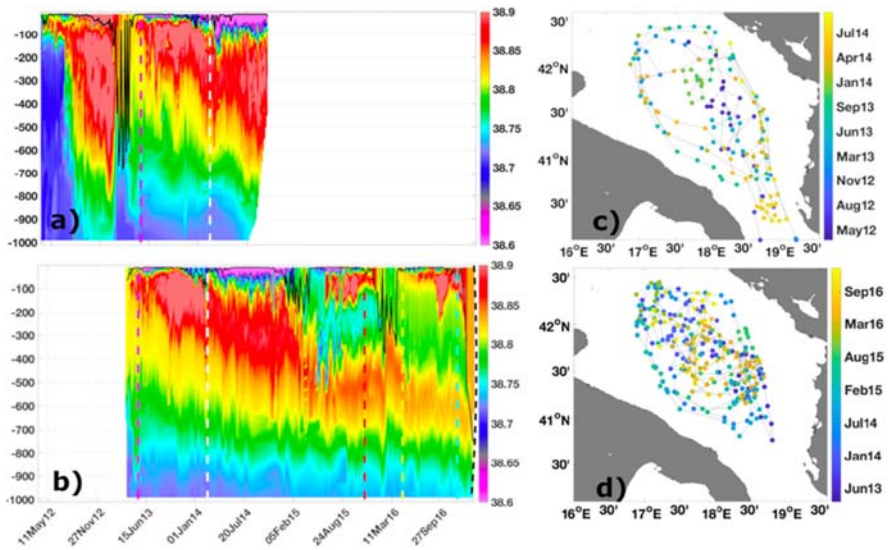

FIGURE 7.9

Hovmöller diagrams of salinity data from Argo floats (A) 6901040 and (B) 6901822 in the southern Adriatic Sea. The corresponding float trajectories are color-coded by time and shown in (C) and (D), respectively. The colored vertical dashed lines depict the time of glider campaigns. The black line indicates the mixed layer depth in (A) and (B).

From Kokkini, Z., Mauri, E., Gerin, R., Poulain, P.M., Simoncelli, S., Notarstefano, G.,n 2020. On the salinity structure in the South Adriatic as derived from float and glider observations in 2013–2016. Deep-Sea Res. Part II 171, 104625.

7.3.2.2 The Aegean Sea as an intermittent deep water source to the eastern Mediterranean

The Aegean Sea has been proposed as a possible source of deep waters for the EMED since the 1950s (Pollak, 1951). However, before 1987 the Aegean Sea was found to be only an occasional and minor contributor to the deep and bottom waters of the EMED (Lascaratos et al., 1999). The Eastern Mediterranean Transient (EMT) event, occurred after 1987, unambiguously defined the Aegean Sea as a source of EMDW. The changes that occurred during the EMT are the subject of Chapter 9, and thus here it is only noted that very cold and dry winds marked the winters of 1991–92 and 1992–93, with heat losses exceeding climatology by about 40% (Josey, 2003). These heat losses are the main cause of the massive formation of dense waters in the Aegean Sea, in particular those in the deep basin of the Cretan Sea. Cretan Deep Water (CDW) underwent a continuous increase in density throughout the 1987–95 period (0.2 kg m^{-3}, Gertman et al., 2006), leading to its overflow through the Cretan Arc Straits, filling the deep and bottom layers of the EMED. Observations demonstrated that by 1996 the CDW signal had penetrated

the Western Ionian Sea. The CDW outflow averaged nearly 3 Sv between mid-1992 and late 1994, and was at its largest during 1993, when Aegean-influenced deep waters extended from the bottom upwards to 400 m depth to the south and west of Crete (Roether et al., 2007).

The Aegean Sea DWF processes have similar characteristics to those of the Adriatic Sea. The Cretan Sea pits are areas of dense, open ocean convection at ∼2000 m, and thus slightly deeper but comparable to the Southern Adriatic pit. The northern Aegean and the Cyclades plateau DWF processes (see Table 7.2) may also contribute to the bottom waters of the Cretan Sea (Velaoras et al., 2021). The Black Sea waters entering from the Dardanelles have approximately the same influence as the river runoff in the Northern Adriatic Sea (Verri et al., 2018), that is, they can shut off the water densification processes.

As Ozer et al. (2020) noted, the Adriatic became again the main source of EMDW in the 2000s, as confirmed in other studies (Manca et al., 2006; Rubino and Hainbucher, 2007; Bensi et al., 2013). Manca et al. (2006) estimated that in 2002 the dense water of Adriatic origin again replenished the volume of the deep Ionian basin by more than 50%.

7.3.3 Formation of intermediate water masses

7.3.3.1 Levantine intermediate water

The LIW water mass is ubiquitous in the Mediterranean basin, and is characterized by a relative maximum in potential temperature and an absolute maximum in salinity in the TS diagram (see Chapter 4). LIW is also known to be a major contributor to the Mediterranean outflow in Gibraltar. LIWEX Group (2003) noted that the DWF in the Rhodes Gyre follows the "recipe" proposed by the MEDOC Group (1970), i.e., the phases of open ocean convection, preconditioning, mixing and spreading. In the preconditioning, the cyclonic circulation is associated with the doming of isopycnals, and the strong increase of surface salinity in summer and fall through evaporation is associated with the northern Etesian winds, which thus explains the high salinity of LIW. This surface increase in salinity is specific to the Levantine Sea area preconditioning. The "violent mixing" phase most frequently occurs in January/February during strong episodes of cold and dry winds. At the end of the mixing phase, the spreading of the newly formed water mass occurs along isopycnal surfaces from the periphery of the convection site toward the various parts of the basin. Although also the formation of deep water (Levantine Deep Water, LDW) has been documented (Sur et al., 1992; Ozsoy et al., 1993; Gertman et al., 1994; LIWEX Group, 2003), the Rhodes Gyre is mainly known to be the main source of the LIW. Other regions of the Levantine basin have also been identified as LIW sources, leading to extensive scatter in the LIW TS characteristics. These include the Antalya Bay in the northern Levantine (LIWEX Group, 2003) and the Turkish coastline to the west of Cyprus in general (Ovchinnikov, 1984), the southern Levantine basin (Hecht et al., 1988) and the Cilician basin. The formation

mechanism in these regions differs from that of the open sea, as it corresponds to the shelf water formation described in the next section.

7.3.3.2 Cretan intermediate water

Schlitzer et al. (1991) identified the CIW mass in the Aegean, which is formed both on the Aegean continental shelves and by open ocean convective mixing in the Cretan Sea (Velaoras et al., 2021). This water mass has variable characteristics although it is close to the LIW and is probably formed in smaller amounts. Millot (2013) reported that the density of CIW compared to that of LIW can depend on the period. In the western Cretan Straits, the intermediate water mass can be extremely variable, which reflects the varying mix of LIW and CIW. Following on from Manca et al. (2006), Millot (2013) estimated that LIW could represent two-thirds to three-quarters of the intermediate waters found at the Sicily Channel, with CIW responsible for the remainder.

7.3.3.3 Western intermediate water

WIW is a cold, low-salinity water mass formed in winter in the WMED and located in the layer between the surface AW and the intermediate LIW/CIW. WIW has a wide range of temperature and salinity, reflecting the different formation zones. This water mass has been commonly observed in the Ligurian Sea and the Gulf of Lion and has been extensively documented in the Balearic Sea. Millot (1999) identified two formation mechanisms, one in the open sea corresponding to winter winds where the cooling is too weak to trigger deep convection, and the other on the Gulf of Lion shelf and the Balearic Sea, which is associated with lower salinities. Pinot and Ganachaud (1999) deduced from a 1993 hydrographic survey that WIW formation could take place on the slope at the edge of the density dome, where convection cannot penetrate deeply because of stratification. Fuda et al. (2000) explained that WIW present near the surface in winter is progressively mixed with warmer AW, while Gasparini et al. (1999) suggested its subduction below the Liguro-Provencal Current. Cold WIW is expected to mainly follow the path of AW along the Spanish coast and across the Algerian Basin (Millot, 1999) but Fuda et al. (2000) proposed another pathway directly southward from the Gulf of Lion to the Algerian basin. Pinot and Ganachaud (1999) noted the recurrent presence of WIW in mesoscale eddies (or Weddies) in the Balearic Sea that strongly affect the general circulation, such as the recurrent obstruction of the Ibiza Channel by a large anticyclonic eddy. WIW was identified by Gascard and Richez (1985) in the Strait of Gibraltar, while Allen et al. (2008) conducted a detailed analysis of a Weddy and speculated that eddy transport toward the Alboran Sea may prove to be the ultimate fate for a significant proportion of WIW. Ben Ismail et al. (2014) observed that WIW is also able to penetrate the EMED through the Sicily Channel. WIW changes have recently been examined (Juza et al., 2019), and positive trends in both temperature and salinity have been found for the WIW, indicating a decrease in density in the most recent period from 2011 to 2015.

7.3.3.4 Tyrrhenian intermediate water

Another intermediate water mass formation area, the Bonifacio cyclonic gyre (Artale et al., 1994), has only recently been proposed (Napolitano et al., 2019). This WIW is called TIW, it sits above the LIW, in the layer between 100 and 200 m, and is characterized by a relative minimum of temperature and salinity in the TS diagram (Napolitano et al., 2019). Fuda et al. (2002) examined observations of Tyrrhenian deep waters and argued that local open ocean DWF can also occur in the Bonifacio cyclonic gyre. However, the evidence is not strong enough and no conclusions about this open ocean DWF region are drawn.

7.3.4 Dense shelf water formation and cascading

Dense waters formed over shelves by cooling and evaporation is a common process in the world ocean (Ivanov et al., 2004). Once it is denser than its surroundings, shelf water sinks and overflows off shelves, a process known as dense shelf water cascading (DSWC). This develops into a near-bottom gravity current that is able to reach the ocean bottom or to form intermediate waters. Cascading is a major contribution to shelf-deep ocean exchange.

These processes have been extensively documented for the Gulf of Lion shelf and the Adriatic, and in various regions of the Aegean Sea. The water masses formed are cold and have low salinity, due to fluvial inputs. They can interact with convection by sinking into deep basins in the open sea and thus change the composition of the bottom waters.

7.3.4.1 Gulf of Lion

Winters with strong cascading in the Gulf of Lion are less numerous than those producing deep convection. The dense shelf water formation in the Gulf of Lion appears to be linked to an anticyclonic atmospheric anomaly in the North Atlantic and a cyclonic atmospheric anomaly over the Baltic Sea, which provides particularly favorable conditions for strong, cold, and dry northerly winds over the Gulf of Lion (Durrieu de Madron et al., 2013, see also Chapter 9). Several years of strong cascading reaching the seafloor have been documented through observations at sea (Canals et al., 2006; Durrieu de Madron et al., 2013) as shown in Fig. 7.10.

The Cap de Creus Canyon located at the southwestern extremity of the Gulf of Lion shelf has been found to be the main conduit for cascading, with near-bottom gravity currents approaching 1 m s^{-1}. In the Gulf of Lion, the volume of dense water reaching the open sea ($\sim$1000 km^3) is one order of magnitude below that produced by open-sea convection. However, cascading can play a more important role in the transfer of matter (carbon, sediment, and pollutants). Durrieu de Madron et al. (2013) estimated the large volume of dense shelf water formed during the winter of 2012 and suggested that a significant proportion of the Gulf of Lion open ocean deep water was composed of dense shelf water cascading, which was entrained in the open ocean convection event that occurred at the same time.

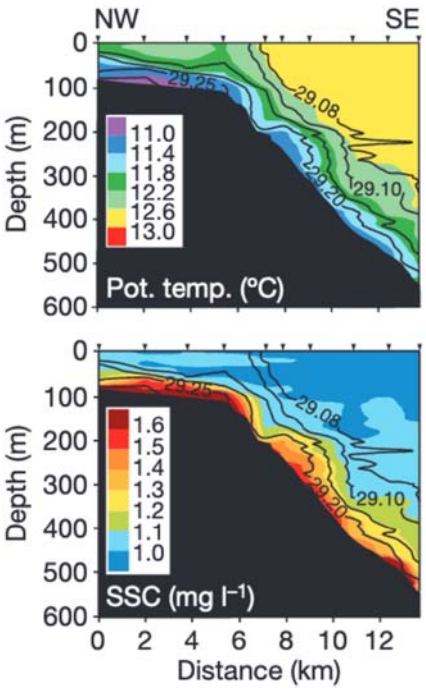

FIGURE 7.10

Potential temperature and suspended sediment concentration measured along the upper part of the Cap de Creus Canyon (potential density anomaly superimposed with black lines). The plume of dense cold water loaded with sediment cascades along the canyon seafloor.

From Canals, M., Puig, P., Durrieu de Madron, X., Heussner, S., Palanques, A., Fabres, J., 2006. Flushing submarine canyons. Nature 444, 354–357.

7.3.4.2 Adriatic Sea

The formation of very dense waters (Northern Adriatic Dense Water - NadDW) on the broad shallow shelf of the Northern Adriatic was identified many years ago (Zore-Armanda, 1963; Artegiani et al., 1997), and Mihanovic et al. (2013) recently reported high-density anomalies in 2012 along the entire eastern Adriatic coastal area, north-west of Split, all of which were above 29.55 kg m^{-3}. They concluded that at least during this exceptional winter, the Croatian shelf areas may be important for DWF and follow the same processes that occur in the Northern Adriatic Sea and other Mediterranean shelf areas. A NAdDW density of up to 30 kg m^{-3} (Vilibic, 2003; Mihanovic et al., 2013) was recorded during severe winters with outbreaks of the cold and dry northeast Bora winds. This is the highest density ever recorded in the whole Mediterranean Sea. NadDW flows as a dense vein along the western Adriatic shelf and escarpment area at a depth of around 50–150 m, cascading in the Middle Adriatic pit, where it rapidly renews old bottom waters (Artegiani

et al., 1997), and in the Southern Adriatic depression (Vilibic and Supic, 2005; Bensi et al., 2013). Turchetto et al. (2007) showed that the Bari Canyon is an efficient conduit for this water mass and associated sediment into the deep Southern Adriatic basin. The NAdDW can occupy the deepest part of the South Adriatic pit with density anomalies of >29.3 kg m^{-3}. Manca et al. (2003) concluded that outflow through the Otranto Strait can be sustained by the contribution of the NAdDW, which fills up the Southern Adriatic dense water reservoir even when deep convection does not occur.

7.4 Theory of dense/deep water formation processes: general concepts

In the following, the conceptual and theoretical models of DWF processes and spreading in the Mediterranean Sea are examined. All symbols in the equations are described in Table 7.3.

DWF processes are associated with a surface increase of water density, due to diabatic exchanges with the atmosphere. Air-sea interactions change the water buoyancy $\left(b = -g\frac{\rho-\rho_0}{\rho_0}\right)$ by buoyancy fluxes, B, written as:

$$B = \frac{g\alpha_T}{\rho_0 C_w} Q_H - \beta_S S_0 g(E - P - R) \tag{7.1}$$

The sign convention in this formulation is that buoyancy fluxes are positive when heat enters the ocean ($Q_H > 0$) and freshening occurs through precipitation and river runoff. DWF is associated with negative buoyancy fluxes that produce "new" waters that have lower buoyancy (higher densities) than those of the underlying layers. Dense waters can become deep waters if several conditions are met, such as if they are dense enough to be gravitationally unstable and force convection.

If only heat losses are considered, and if it is assumed that they are distributed in a layer Δz balanced by turbulent diffusivity, then the following is obtained:

$$K_v\frac{\Delta\rho}{\Delta z} = \frac{-\alpha_T}{C_W} Q_H \text{ or } Q_H = -K_v\frac{\Delta\rho}{\Delta z}\frac{C_W}{\alpha_T} \tag{7.2a, 7.2b}$$

By using (7.2) for a change of density of $\Delta\rho = 0.2$ kg m^{-3} in a layer of 100 m and with a vertical diffusivity of 0.01 m^2 s^{-1}, a heat loss of about -390 W m^{-2} is required, which is a typical winter-time heat loss in several DWF regions of the Mediterranean. Thus, dense waters are "winter waters" that in the subsequent seasons are found either at the bottom or at intermediate depths or disappear due to positive buoyancy gains. At least eight areas of DWF occur in the Mediterranean Sea, as previously described (including four shelf areas).

The question of how dense waters reach the sea bottom is more challenging. Dense waters can become deep or bottom waters through different processes. First, in open ocean convection, newly formed dense waters directly reach the bottom

Table 7.3 Symbols, units, and values of the parameters used in the text.

Symbol	Units	Description	Typical value in the Mediterranean sea
ρ	kg m^{-3}	Seawater potential density	[1027.5 – 1029.3]
ρ_o	kg m^{-3}	Reference constant density value	1000
f	s^{-1}	Coriolis parameter at 40N	9.410^{-5}
β	m^{-1}s^{-1}	Beta parameter at 40N	1.810^{-11}
H	m	Depth of open ocean convection	[1000 –2500]
B	m^{2}s^{-3}	Buoyancy flux	$[5.10^{-9} - 30.10^{-8}]$
$\vec{\tau}_w$	N m^{-2}	Wind stress	[0.02 – 0.1] for module
C_W	J kg^{-1}K^{-1}	Specific heat at constant pressure	3900
α_T	K^{-1}	Coefficient of thermal expansion	2.10^{-4}
β_S	−1	Coefficient of haline contraction	7.610^{-4}
K_v	m^{2}s^{-1}	Turbulent diffusion coefficient during the violent mixing phase	0.1 – 10
Q_H	W m^{-2}	Heat flux during winter in DWF areas	[−100, −1000]
$\mathrm{curl}\left(\vec{\tau}_w\right)$	N m^{-3}	Curl of the wind stress	$[2 - 710^{-7}]$
g′	m s^{-2}	Reduced gravity	10^{-4} for almost unstratified plume
L_ρ	m	Reduced gravity Rossby radius of deformation	10^4
N	s^{-1}	Brunt-Vaisala frequency	$[0.8 - 4\ 10^{-3}]$
u_{rim}	m s^{-1}	Rim velocity	0.1

layer in the region where they are formed. Second, through down-sloping or cascading from the shelf area dense waters can reach the abyssal regions as bottom currents. These two different processes must be separately examined.

7.4.1 Theory of dense/deep water formation in the open ocean

Theories regarding the DWF processes in the open ocean regions were proposed immediately after the previously described MEDOC Group (1970) mission in the WMED. The early works of Anati (1971), Killworth (1976), and Gascard (1973, 1978) identified the different phases of the process before the idealized numerical models were developed in the 1990s (Legg and Marshall, 1993; Send and Marshall, 1995; Madec et al., 1996; Marshall and Schott, 1999; Straneo and Kawase, 1999). Here the study by Marshall and Schott (1999) (hereafter MS99) is considered, to provide the main overview of theories about the DWF processes in the open sea.

MS99 subdivided the processes of open ocean DWF into three phases (Fig. 7.11): (a) preconditioning occurs at the scale of a cyclonic gyre circulation (the order of 100 km), where a "dense water patch" (what was previously referred to as the

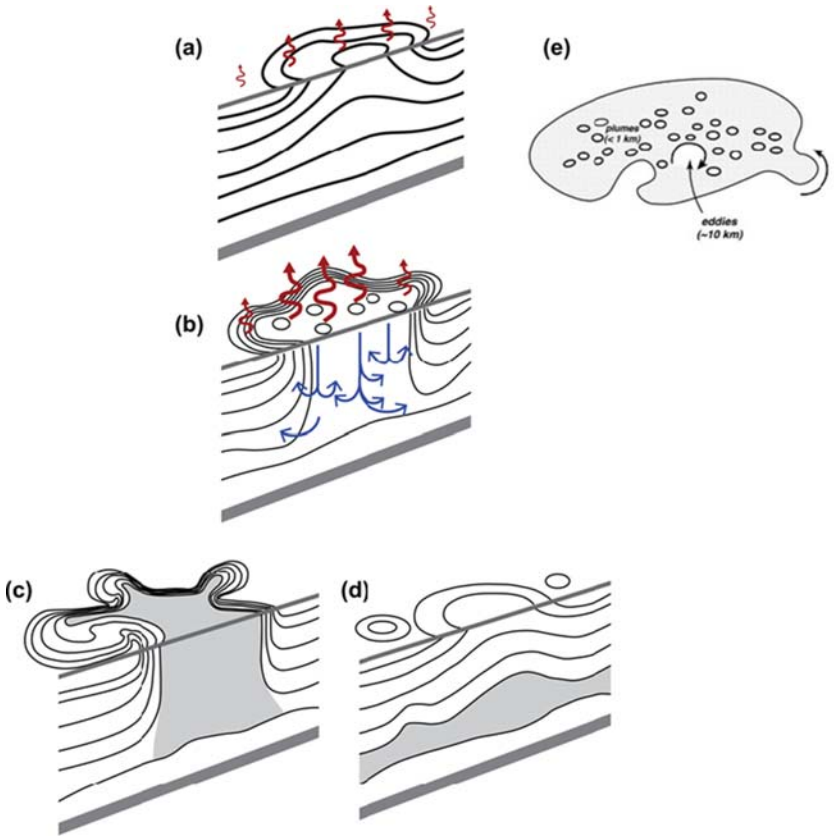

FIGURE 7.11

Phases of the dense/deep water open ocean formation processes and scales of relevance for the overall mechanism of formation of open ocean convection: (A) preconditioning with the isopycnals outcropping in the center of a cyclonic gyre with an intense rim current; (B) violent mixing phase where large buoyancy losses occur and mix the water column; (C) the patch of dense water formed (gray area), the instabilities of the rim current (meanders) that stop convection by fluxing heat inside the area, and with the isopycnals slanted laterally with a net downward motion at the periphery and dense water exiting at depth from the convection area; (D) stratification is reestablished and the newly formed dense water (gray area) is now separated from the surface, ventilating the deep layers; (E) shows the different horizontal scales of motion during the violent mixing phase (the patch of dense water in gray is populated by plumes <1 km and mesoscale eddies of ~ 10 km, originated by the instabilities of the rim current or entrained from outside the patch).

Redrawn from Marshall, J., Schott, F., 1999. Open-ocean convection: observations, theory, and models. Rev. Geophys. 37 (1), 1–64.

"chimney" area, but after the discovery that the net vertical velocity is zero at the center of the dense water area, it is preferable to use "patch" to indicate the newly formed dense water area) can form by convection; (b) the violent mixing phase or deep convection is characterized by scales of "plumes" (the order of 1 km) inside the patch; and (c–d) the lateral exchange and spreading phase occurs at the mesoscale (the order of 10 km or more in the Mediterranean Sea) produced by instabilities of the rim current at the border of the patch.

The preconditioning phase at the cyclonic gyre circulation scale characterizes all of the dense/deep water open ocean areas. This was examined in detail by Madec et al. (1996) (hereafter MLDC96) in the northern WMED formation area, by taking a mechanistic numerical modeling approach. The simulation was conducted with specific air-sea forcing and simplified geometry. No equivalent process study has been conducted on other open ocean DWF areas in the Mediterranean Sea. MLDC96 established that the wind-driven circulation in the northern WMED produces a preconditioning cyclonic gyre that is not necessarily of the same size as the dense water patch, and that in the open ocean is dominated by the Sverdrup balance, that is,

$$\beta vH = \frac{1}{\rho_0} \mathrm{curl}\left(\vec{\tau}_w\right) \tag{7.3}$$

Given that the winds of this area have an important northerly component, $\vec{\tau}_w \sim \left(0, \tau_w^{(y)}\right)$ and using the barotropic velocity stream function $vH = \frac{\partial \psi}{\partial x}$, it is possible to estimate the maximum value of the barotropic stream function field in the preconditioning gyre as:

$$\psi_{max} = \frac{1}{\rho_0 \beta} \max\left(\tau_w^{(y)}\right) \approx 5 - 10 \text{ Sv} \tag{7.4}$$

The value is slightly higher than those calculated using complex realistic models (Pinardi et al., 2015), but is of the correct order of magnitude. Thus, in the Mediterranean the dense water preconditioning gyre is a wind stress curl forced gyre, as suggested by MLDC96 and Pinardi and Navarra (1993). The buoyancy forcing has little or no impact on the preconditioning gyre strength.

This preconditioning gyre is characterized by a rim current of the order of few tens of cm s^{-1}, as implied by Eq. (7.3) for the maximum wind stress curl values of the Mediterranean Sea given by Pinardi et al. (2015) and reported in Table 7.3. MLCD96, noted that the buoyancy forcing and the thermohaline structure of the gyre add two other important factors: weak stratification at the center of the gyre and the baroclinic instability process of the rim current, which is active during the third phase of the process, that is, the lateral exchange phase.

MLCD96 also demonstrate the importance of the "Rhone fan," which is a bathymetric feature that constrains the local flow, as shown in the realistic bathymetry of Fig. 7.12.

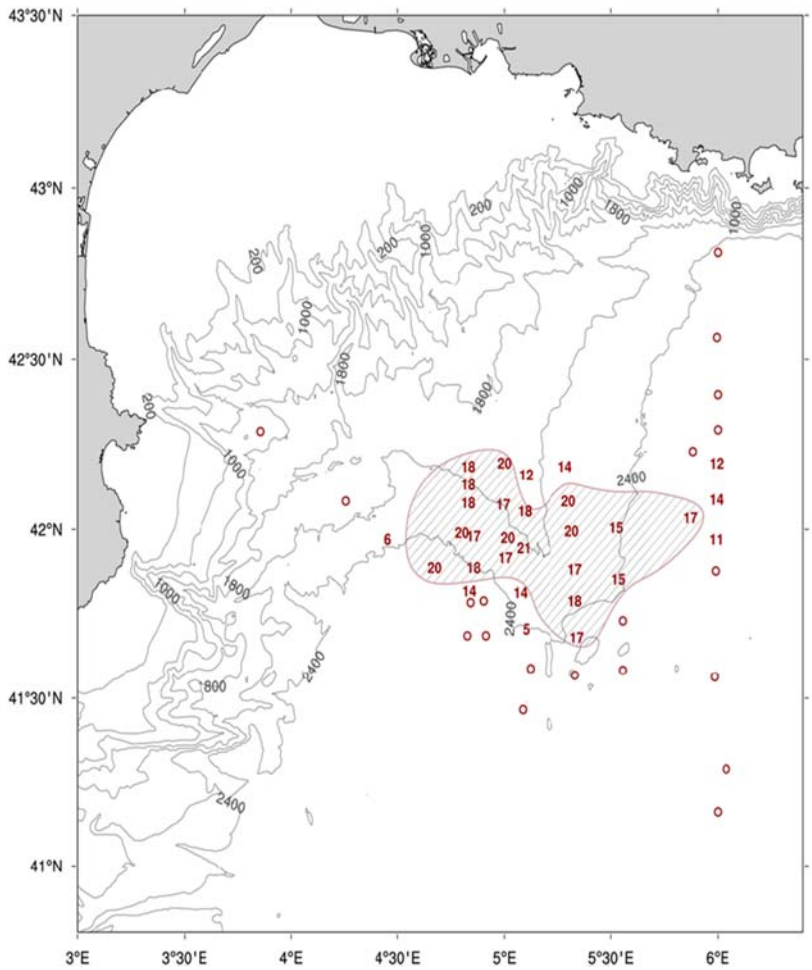

FIGURE 7.12

The "Rhone fan" geometry in the area of DWF in the northern WMED. The fan is characterized by the shape of the bathymetric isoline of 2400 m. The numbers on the shaded patch indicate the depth of the temperature mixed layer in units of 100 meters. The stations were collected between 16 and 21 February 1969.

Redrawn from Swallow, J.C., Caston, G.F., 1973. The preconditioning phase of MEDOC 1969. Part I. Observations. Deep-Sea Res. 20, 429–448.

The cyclonic preconditioning gyre within the Rhone fan is smaller and closely resembling the final dense water patch (Fig. 7.13). Thus, both wind stress curl and bathymetry are important in controlling the preconditioning gyre for open ocean DWF. This basic preconditioning feature appears to be valid (Lascaratos et al., 1993)

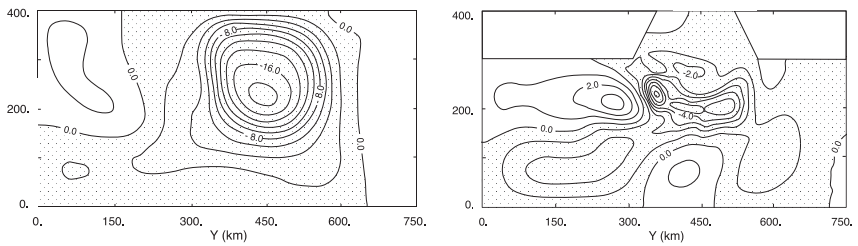

FIGURE 7.13

The wind driven cyclonic circulation for the north-western Mediterranean: left panel, the barotropic streamfunction for the flat bathymetry case; right panel, the barotropic streamfunction for an idealized bathymetry with the Rhone fan. Units are Sv. From MLDC96.

for the other open ocean areas of DWF, i.e., areas 4, 2 and 1 in Fig. 7.3, although no similar studies have been conducted in these regions.

Send and Marshall (1995) (hereafter SM95) described in detail the deep convection/violent mixing phase dynamics in the Mediterranean open ocean areas. This phase is characterized by downward water motion, that is, a negative vertical velocity w, which has been measured to be as much as 10 cm s^{-1} (Schott and Leaman, 1991) as shown in Fig. 7.7. How can such a high vertical velocity occur in this deep convective patch? If net downward motions of this intensity were created in the mixed patch, the induced vorticity and rim current speed would be several orders of magnitude larger than that found through laboratory and numerical experiments. The explanation given by SM95 provides some insights. The space scale of the convection inside the patch is connected to "plumes" that can be understood as 1 km diameter cylinders that mix water vertically. Plumes are very rapid overturning cells with upward and downward vertical velocities that almost compensate for each other, with each having both descending and ascending branches. The vertical velocity associated with the plumes was found by Jones and Marshall (1993) to be:

$$w_{plume} = \sqrt{\frac{B}{f}} \tag{7.5}$$

where B is the buoyancy flux and f is the Coriolis parameter. With $B = 5\ 10^{-7}$ m^2 s^{-3}, corresponding to heat losses of 1000 W m^{-2}, 7 cm s^{-1} is obtained. This is consistent with the measured downward vertical velocities, but there are equivalent upward vertical velocities in the plumes, so that in the area of the mixed patch the net vertical velocity is close to zero. Margirier et al. (2017), shown in Fig. 7.7, found in the northern WMED a prevalence of downward velocities in the mixed patch, but this may be due to the limited observational sampling of the area. Waldman et al. (2018) examined the sampling error to estimate the volume of water formed in the northern WMED and found it to be of the order of 20% −25%, which can also apply to the distribution of upward and downward vertical

velocities. Spall (2003) conducted a theoretical study of DWF in a marginal sea, and found that a net downwelling motion was only present at the periphery of the cyclonic preconditioning gyre. Thus, the dense water patch does not have a uniform downward vertical velocity. The vertical velocity is in the plumes and the net is almost zero.

MS99 developed the scaling for the diameter of the plumes as:

$$L_{plumes} = \sqrt{\frac{B}{f^3}} \tag{7.6}$$

which then amounts to 600 m for the largest values of B given in Table 7.3. This value has recently been verified by the glider experiment of Margirier et al. (2017), who also reported that the plumes were separated by about 2 km.

The plumes containing dense waters reach the bottom and then collapse under gravity and rotation, giving rise to a geostrophically adjusted well-mixed patch. This collapse has been extensively examined in idealized and laboratory experiments, such as in the studies of Dewar and Killworth (1990) and Maxworthy and Narimousa (1994). The dense water cylinders formed by convection in the chimney slump the interface laterally over a Rossby radius distance $L_\rho = \frac{\sqrt{g'H}}{f}$, that is, the baroclinic Rossby radius of deformation (g' is the reduced gravity and H is the scale height of the stratification). The chimney area then looks like a "cone" with bottom waters moving outwards.

At this point the third phase of the process starts and the baroclinic rim current, enclosing the patch of dense well-mixed waters, becomes unstable and forms mesoscale eddies that contain "dense water cones" and spread apart with time. The dense water at the bottom of these eddies attempts to spread out even further and is only contained by rotation. The eddies are markedly cyclonic at the surface (less at depth), and are efficient at exchanging heat laterally, thus restratifying the cold-water mixed patch in about one week. Straneo (2006) detailed the final process of lateral heat exchange through eddies, which balance the heat loss during the violent mixing phase, fluxing heat laterally into the well mixed patch. In this phase, the restratification of the mixed patch is mediated by the eddies.

SM95 treated the instability of the rim current as an Eady instability problem, and examined continuous buoyancy loss over 6 days. They analyzed the development time of eddies along the rim current. They found that the time scale corresponding to the rim current wave amplification was approximately 3−5 days. The Eady wave along the rim becomes nonlinear and eddies pinch off the patch. The spreading phase continues for months, as eddies propagate away from the mixed patch where vertical stratification is restored. Each region of formation in the Mediterranean Sea has different eddy pathways (this will be discussed in Section 7.5, focused on numerical modeling).

The southern Adriatic Sea is a special case of open ocean convection. This is a deep marginal sea (maximum depth of ∼1200 m) connected to the Ionian Sea by the relatively narrow Strait of Otranto (Fig. 7.3). Unlike other open ocean convection

areas that are unbounded in the horizontal direction, the preconditioning cyclonic circulation is constrained by the geometry of the coasts and by the inflow/outflow system at the Strait of Otranto. In this marginal sea the net buoyancy loss is ultimately balanced by advection through the Strait of Otranto. Spall (2003, 2004) (S04 hereafter) and Iovino et al. (2008) (ISS08 hereafter) investigated a dense/deep water mass transformation process in a marginal sea with the inflow/outflow system at the Strait and a sill, which is very similar to the southern Adriatic Sea convection problem.

S04 confirmed that the net vertical velocity in the patch of well-mixed, dense water formed by buoyancy losses was zero, and that downwelling was present at the boundaries of the domain, where boundary currents sit along the bathymetry slope. The ratio of the isopycnal slope to the bathymetry slope is the key parameter for quantifying the exchange between the well mixed patch and the unstable boundary current during the last phase of convection. Thus, fully open ocean dense/deep convection differs from marginal sea open ocean deep water convection in the last phase of the process, during the lateral exchange and restratification, and during spreading. ISS08 examined the effect of the addition of a sill in the marginal sea and found that the temperature of the well-mixed patch of water was lower than without a sill, as the inflow of warm waters by the boundary currents around the basin is affected (Fig. 7.14). The greater density of the deep waters of the EMED compared to the WMED may be due to this, and the deep waters of the Adriatic and Aegean Seas may be denser than the WMDW because they are formed in deep marginal seas with sills.

7.4.2 Dense water formation on the shelf and their cascading into the deep ocean

Dense waters on the shelf are formed as in the open ocean through extensive buoyancy losses during winter. The process of dense water preconditioning for the shelf areas differs from that of the open ocean due to lateral and vertical geometrical constraints. The nearby land-derived runoff and precipitation are also important factors that can modify the preconditioning processes and the final dense water volume. The spreading phase is also very different because it involves cascading: this is a specific type of buoyancy-driven current in which the dense water formed over the continental shelf descends along the continental slope to a greater depth.

Shapiro et al. (2003) (SHI03 hereafter) proposed a three-stage process of dense water cascading from shelves: the dense waters form on the shelf; they are transported to greater depths (plumes and bottom density currents); and finally the cascading waters mix with the ambient waters.

In the first phase, a homogeneous patch of dense water forms on the shelf directly down to the bottom because the convection depth is typically greater than the shelf depth, and thus the dense water occupies the whole shelf volume. With the same level of cooling and evaporation at the surface, the shelf waters will be heavier

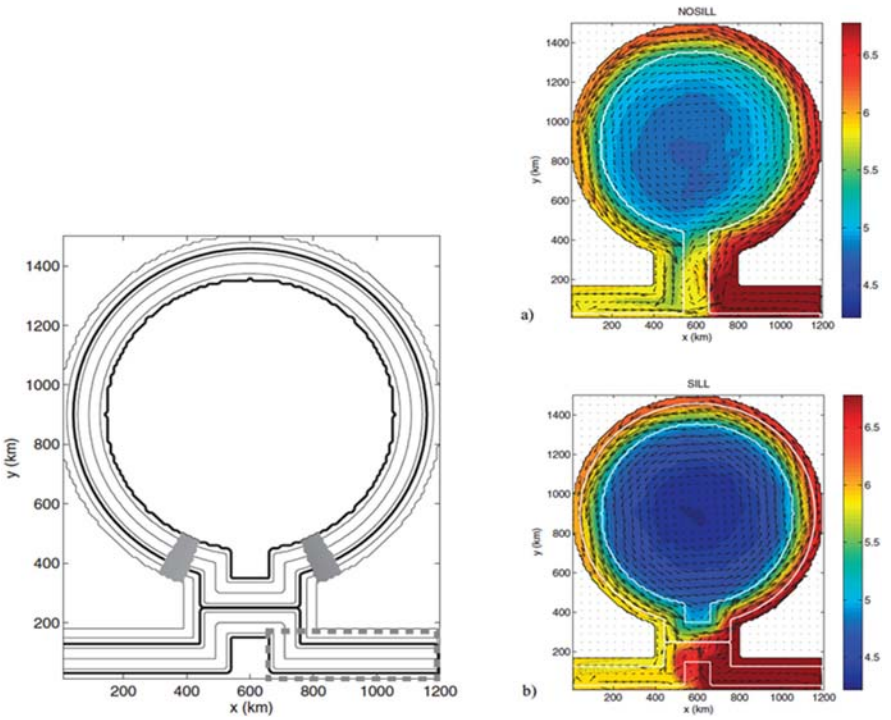

FIGURE 7.14

Left panel: the idealized geometry of the dense/water formation numerical simulation domain for a marginal sea with a sill at the entrance but with a deep basin in the semienclosed area. The center of the marginal sea is cooled to produce the well-mixed patch while the boundary current entering and outflowing is baroclinic and produces eddies. (a) and(b) panels on the right: temperature field in the basin with (b) and without (a) sill

From ISS08.

than the offshore waters. The density difference between the shelf and the offshore waters is:

$$\frac{d\rho}{\rho_o} = \frac{\rho_c - \rho_s}{\rho_o} = \left(\beta_S \frac{dS}{dz} - \alpha_T \frac{dT}{dz}\right) \frac{(H_c - H_s)^2}{2H_s} \tag{7.7}$$

Some of the symbols are explained in Fig. 7.15. This theory is valid without considering the advection of salinity on the shelf. The dense waters are transported from the shelf after the first phase of dense water and density gradient formation. The cross-shelf distance over a slope S is indicated by L, and thus SHI03 find that

$$R_H = \frac{d\rho}{\rho_0} \frac{S\, g}{L\, f^2} > 1 \tag{7.8}$$

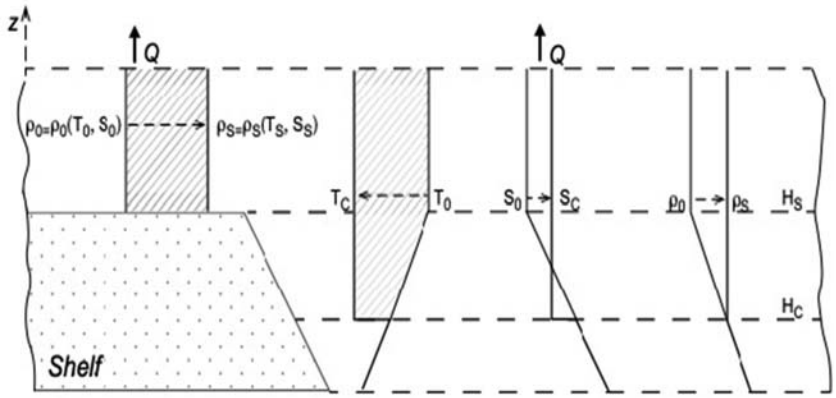

FIGURE 7.15

Scheme of formation of horizontal density contrast between shelf and slope waters under identical outward heat flux. Subscripts 0, S and C denote the initial state, shelf water and slope water, respectively.

From SHI03.

is the necessary condition for the start of the time-dependent shelf-water cascading process. If the density gradient is not strong enough or if the slope is too small compared to the across-shelf density contrast distance L, cascading will not occur. Several regimes of dense water downslope transport have been observed, from a broad and thick plume dominated by geostrophy to an unstable along-slope current that will transport the waters away by eddies. The bottom Ekman layer thickness is also a controlling factor for the shape of the downsloping plume, and if the plume is thicker than twice the bottom Ekman layer depth $H_E = \sqrt{\frac{2K_v}{f}}$, the plume has a nose and a complex shape. The cascading process can last several months and have been estimated to be 6–7 months in some conditions, and thus remnants of shelf dense waters plumes can be found during the summer. In the Mediterranean Sea, dense water cascading occurs from the areas in the Cyclades Plateau, the Northern and North-Eastern Adriatic and the Gulf of Lion shelves (areas 3, 5, 6, and 8 in Fig. 7.3).

After the initiation of cascading, the density and volume of the plume are modified by mixing with the ambient waters, thus entering the third phase. During this phase the plume finds its buoyant layer and it detaches from the bottom, intruding into the ambient waters. An interesting outcome of (7.7) is that the maximum depth of intrusion H_{max} of dense waters can be written as (the symbols are defined in Fig. 7.15):

$$H_{max} = H_c + \frac{H_s}{2}\left(\frac{H_c}{H_s} - 1\right)^2 \tag{7.9}$$

For the northern WMED, assuming the depth of open ocean convection to be 1000 m and the shelf depth to be 200 m, the maximum depth of intrusion will be

2600 m, that is, the bottom of the Gulf of Lion area. For the northern Adriatic, assuming a shelf of 30 m and a convective process in the Middle Adriatic of 100 m, the dense water plume will descend only to 180 m. For the Cyclades Plateau, assuming a depth of the shelf of 200 m and an offshore convection depth of up to 500 m, the depth of cascading is 725 m. These estimates are only valid if during the first phase of cascading there is no advection of ambient waters on the shelf. Dense water cascading is thus an efficient method of ventilating the deep layers of the ocean in the offshore areas of the Mediterranean Sea, even below the depth of the open ocean convection process.

7.5 Numerical modeling of deep/dense water formation

In this section, the reconstruction of DWF events and processes in the Mediterranean Sea using numerical models with realistic geometry is presented. In the previous section, it was noted that the geometry of the subbasins in the Adriatic and Aegean Seas is important for DWF in semienclosed seas, as it differs from that in the open ocean. The WMDW may also depend on continental escarpment structures such as the "Rhone fan" (Fig. 7.12) that affect the preconditioning phase of DWF. As previously discussed, the DWF on the shelf depends on the shelf bathymetry. Finally, the spreading phase of dense/deep waters depends on the specific bathymetry, such as the funneling effect of canyons in dense shelf water cascading. Thus it is important to use realistic bathymetry and geometry to understand and reproduce the observations.

Attempts at realistic modeling first began in the 1990s, when numerical models based on primitive equations first achieved eddy resolution and included adequate physical representations of mixing. These models were mainly aimed at characterizing the buoyancy forcing that triggers the DWF processes, the interactions between water masses formed in different parts of the basin, the spreading phase of deep convection and the climate trends in water formation rates. First the open ocean convection will be discussed, and then the shelf dense water cascading simulations.

7.5.1 Dense/deep water formation numerical modeling in the open ocean

The first numerical DWF simulations in the WMED were conducted by Madec et al. (1991) within an idealized context. A realistic geometry and bathymetry simulation throughout the Mediterranean was then conducted by Castellari et al. (1998, 2000). The air-sea buoyancy fluxes required to obtain the heat and water losses favorable for DWF to occur were taken particularly into account in these simulations. Several numerical artifacts were required to produce the observed features of the formed deep water (particularly for the salinity boundary conditions) because the primitive equation model and the atmospheric forcing variables were of relatively coarse resolutions in both the horizontal and the vertical (0.25° lat $\times$ 0.25° long and 31

vertical levels for the ocean model). The atmospheric forcing variables were also coarse in space and time (12 h atmospheric forcing analyses on a 1° lat × 1° long grid). The results confirmed that open ocean convection could be simulated in a realistic basin-scale ocean general circulation model of the Mediterranean Sea with calibrated buoyancy fluxes.

These early results also indicated the importance of salinity in the preconditioning of the convection depth, but raised the question of how salt accumulates in the dense/deep ocean areas and whether it affects the formation process. In the Mediterranean Sea, surface salinity increases locally through basin-scale summer and event-intense winter evaporation events, and also through the advected subsurface salinity maximum corresponding to LIW. Wu and Haines (1996) investigated the problem of connecting the advection of intermediate, salty waters to the DWF mechanisms in the Mediterranean Sea. They indicated that the advection of LIW partially drives the specific DWF processes in the Adriatic and WMED by increasing the density, thus leading to convection at greater depths. Thus, it is concluded that salinity not only increases locally through summer evaporation and winter buoyancy fluxes, but it is also advected from remote regions, thus affecting the local DWF processes.

Around the same time, the EMT (Roether et al., 1996 and Chapter 9) captured the attention of the numerical modeling community who examined the EMT phenomenon. Wu et al. (2000) performed realistic numerical simulations of the entire Mediterranean Sea and found that the CDW was associated with a salinity redistribution process and was triggered by intense cooling events over the Aegean Sea. The salinity redistribution process is connected to changes in LIW path that lead to the accumulation of salt at the subsurface in the Cretan Sea, but the intense and repeated large buoyancy losses in the Aegean Sea are the final trigger of the deep water convection in the Cretan Sea. Nittis et al. (2003) obtained numerical simulations for the EMED realistic geometry for a period of ∼15 years and demonstrated not only the significance of buoyancy losses over the Aegean Sea, but also the uniqueness of this event, which formed 0.2−0.3 Sv of dense and deep waters. The latest numerical simulations of the EMT (Beuvier et al., 2012) confirmed the triggering effect of atmospheric forcing conditions using a much higher resolution model of the Mediterranean Sea and more accurate atmospheric forcing.

The latest attempt to simulate the open ocean convection processes in the Adriatic Sea with a realistic general circulation model was conducted by Verri et al. (2018), encompassing the entire central Mediterranean Sea. They addressed the effect of the large river runoff of the Adriatic Sea basin on the DWF in the southern basin. They found that the open ocean DWF processes were marginally affected by river runoff changes and that wind and buoyancy fluxes were the dominant controlling factors for AdDW formation processes, in addition to the semienclosed basin geometry. While the southern Adriatic DWF process may also occur in years of large river runoff, the amount of deep water formed was found to be affected by the freshwater inputs and by dense water cascading from the middle and northern Adriatic regions.

For most of the water masses shown in Table 7.2, Pinardi et al. (2015) examined the rate of formation through the first reanalysis of the Mediterranean Sea (Adani et al., 2011). The reanalysis data-sets are the basis of the study of realistic deep water simulations, as they encapsulate the observations and the dynamic numerical model interpolation/extrapolation. The analysis showed that in the various open ocean DWF regions shown in Fig. 7.3, the formation processes occur over 3−5 years, after which they remain low for a comparable length of time, suggesting that there is multiyear memory in the process, which is yet to be fully understood. This is also shown in Fig. 7.6, which illustrates the most recent reanalysis of the Mediterranean Sea climate (Escudier et al., 2021).

The latest attempt to simulate the complex dynamics of WMDW processes over a long time period (1980−2013) was conducted by Somot et al. (2018) using a combined ocean-atmosphere model. They found that the model reported deep convection (deeper than 1000 m) in 22 of the 33 winters over this period, corresponding to an average DWF rate of ∼0.3 Sv, with a strong interannual variability and a maximum value of ∼1.7 Sv in 2013 and 2005.

Estournel et al. (2016b) focused on specific large formation events, like that of 2012−13, and demonstrated that with precise initial conditions and atmospheric flux time series, oceanic convection is predictable over several months. However, they focused on two key processes that affect the buoyancy budget of the convection zone during the preconditioning and convective phases, such as the direction of the wind with respect to the frontal area in the ocean. When the wind blows in the same direction as the current associated to the front (downfront wind), destratification is produced at the submesoscale through the Ekman buoyancy flux, which is the product of the Ekman transport and the horizontal surface buoyancy gradient. Seyfried et al. (2019) showed that = in the Gulf of Lion the stratification variations in the vicinity of the Northern Balearic front (separating the warm and fresh AW from the colder and saltier water present in the center of the Gulf of Lion cyclonic gyre) are principally driven by the Ekman buoyancy flux. Bosse et al. (2021) examined this process in winter, and they identified remarkable layers of negative potential vorticity in the upper 100 m on the dense side of fronts surrounding the deep convection area along the Northern Current. During winter, and particularly during the convection phase, lateral advection tends to restratify surface waters. Estournel et al. (2016b) used a 1-km horizontal resolution model and suggested that during convection, much of the buoyancy forcing works against the restratification effects of the lateral advection intensified by the intermittencies of surface forcing (wind and associated surface buoyancy fluxes). Waldman et al. (2017) evaluated the significance of ocean internal variability (mesoscales) in the water mass formation area extension and DWF rate in 2012−13 through a comprehensive numerical simulation study. They identified a relatively low impact during the preconditioning and violent mixing phases, but as expected, the impact was greater in the spreading phase.

The spreading phase of open ocean DWF events has only been examined using numerical simulations, as newly formed waters must be followed for several months after their formation. Demirov and Pinardi (2007) analyzed the relationship between

eddy transport and pathways for the 1987 and 1992 WMDW events. They found that in the 6 months following the convection event in 1987, a large amount of newly formed deep water remained confined to the Gulf of Lion gyre. At the end of summer, the southern rim of the Gulf of Lion gyre begins to break down and forms eddies (diameter $\sim$ 100 km) that transport the deep waters away from the formation regions. Such eddies interact and merge later with other eddies of the Algerian basin. Demirov and Pinardi (2007) concluded that the spreading of the WMDW is dominated by the eddy processes of the Algerian basin, which disperse the newly formed deep waters westward toward the Gibraltar Strait.

Beuvier et al. (2012) recently conducted another numerical modeling study of deep water spreading for the WMDW event of 2005. They again found that at the end of summer several deep cyclones were mainly responsible for the rapid spreading of the WMDW southwards in the WMED. These cyclones also encourage the propagation of the WMDW toward the Channel of Sardinia and possibly decrease the volume of WMDW that can reach the Strait of Gibraltar.

Finally, Damien et al. (2017) conducted a realistic simulation of intermediate and deep convection events in the Gulf of Lion, and identified for the first time the formation of Submesoscale Coherent Vortices with a radius of $\sim$6 km. The long lifetimes (several months) of these anticyclonic and cyclonic eddies reflect a slow diffusive process between their core and the surroundings. These SCVs help to spread a significant proportion (from 15% to 35%) of the convected waters in the Gulf of Lion and contribute to the ventilation of the deep basin.

7.5.2 Dense/deep water cascading numerical modeling

In the following an overview of the numerical modeling of dense water cascading from the Gulf of Lion shelves (area 9 in Fig. 7.3) and the Northern Adriatic shelf areas (areas 5 and 6 in Fig. 7.3) is provided.

Dufau-Julliand et al. (2004) simulated area 9, where dense coastal water form. Their analysis demonstrated that the down-slope motion of the plume is only partially explained by the friction effects and Ekman drainage. Local effects, such as the sharp bottom topography or coastline shape, also lead to the nonnegligible forcing of the down-slope motion. The presence of the Lacaze-Duthiers and Cap Creus canyons in the study area probably causes the breaking of the geostrophic constraint. Ulses et al. (2008) analyzed the 2005 cascading event and provided the reproduction of the water mass properties and the amount of water transported off the shelf, showing that it contributes to the renewal of the WMDW.

Wang et al. (2006) modeled the NAdDW cascading into the southern Adriatic Sea. They showed that the NAdDW bottom density plume cascades from the Gargano peninsula (located approximately at 42° N on the Italian coastlines) arrive there along the western Italian shelf, with a propagation speed of 0.1 m s^{-1} and a down-slope component of the order of 0.05 m s^{-1} at the Gargano peninsula. The connection between the interannual variability in the Gargano bottom density plume and the production of NAdDW constitutes an important finding in this work. The

numerical study demonstrated that a continuous heat loss of 175 W m^{-2} from November to January is required to produce an adequate volume of NAdDW, so that the density anomaly is strong enough to drive a density current that reaches the Gargano Peninsula in the spring and then cascades into the southern Adriatic deep basin .

7.6 The Mediterranean overturning circulation: structure and dynamics

Like the overturning circulation of the global ocean, which plays a key role in setting the stratification of different basins and transporting oxygen and other tracers from the surface to the deep ocean, the Mediterranean overturning circulation is key to provide low salinity waters to the Mediterranean as it balances the salt increase associated with the net evaporation inside the basin and determines the basin's stratification.

The Mediterranean overturning circulation is fed by the two-layer flow at the Gibraltar Strait. The potential energy associated with the Gibraltar Strait flow balances the surface wind-work and buoyancy flux (Cessi et al., 2014), thus providing energy to the overturning cells. The geometry of the Mediterranean Sea (Fig. 7.3), reveals several sills shallower than 500 m that divide the basin into several subbasins. The major subdivision occurs at the Sicily Channel, which separates the WMED from the EMED.

The zonal overturning cell that connects the two-layer flow at the Strait of Gibraltar to the EMED is limited to the surface and intermediate waters exchanged at the shallow Sicily Channel (Pinardi et al., 2019). However, within the EMED there are deeper circulations associated with DWF in the Adriatic and the Aegean Seas. The geometry of the basins and the large winter buoyancy losses in these semi-enclosed seas enables DWF, as explained earlier.

In addition to the zonal overturning cell that spans the Mediterranean from the Gibraltar Strait to the eastern end of the EMED, two primarily meridional deep cells occupy the WMED and the EMED. The WMED overturning circulation is connected to the DWF areas of the Gulf of Lion. The EMED meridional overturning is connected to the Rhodes Gyre, Aegean Sea, and Adriatic Sea DWF areas (Pinardi et al., 2019).

7.6.1 Zonal overturning

Wüst (1961) mapped the zonal overturning circulation (ZOC) by following water masses in the basin using the "core method", that is, tracking the positions of extremes in temperature, salinity and oxygen (see more on this in Chapter 4). A tongue of high salinity was identified along a longitudinal section spanning from the eastern end of the EMED to the Gibraltar Strait, which emanated from the EMED below a low-salinity tongue from the Gibraltar Strait.

A modern dataset supplemented by a dynamically consistent eddy-resolving model that assimilates observations (Simoncelli et al., 2017) can provide a quantitative estimate of the ZOC. The ZOC can be calculated in either vertical-longitudinal or density-longitudinal space. The transport of volume is quantified in the vertical-longitudinal space, which is the zonal equivalent of the classical Eulerian Meridional Overturning Circulation (MOC).

The overturning in density space quantifies the transport of buoyancy and is associated with the residual circulation, defined as:

$$\psi^{*}_{zon}\left(x,\widetilde{\sigma}\right)=\frac{1}{T}\int_{t_0}^{t_1}\int_{y_{B1}}^{y_{B2}}\int_{-H}^{0}\mathscr{H}\left[\widetilde{\sigma}-\sigma(x,y,z,t)\right]u(x,y,z,t)dzdydt \tag{7.10}$$

where $\mathscr{H}$ is the Heaviside function and σ is the potential density (Young, 2012). The zonal circulation is illustrated in Fig. 7.16 (Pinardi et al., 2019). The Eulerian overturning (upper panel) shows a shallow clockwise cell spanning the whole basin in longitude, corresponding to the circulation identified by Wüst using the "core method." Additionally, a counterclockwise cell dominates the WMED below 700 m, while multi-centred clockwise cells extend to the bottom in the EMED. These clockwise cells are associated with deep water outflow in the Aegean and with DWF in the Rhodes gyre.

The WMED deep counterclockwise residual overturning (see the lower panel of Fig. 7.16) is stronger than its Eulerian counterpart, indicating that transport by stationary gyres and eddies reinforces the mean abyssal vertical circulation. The residual cross-isopycnals flow indicates that diapycnal mixing is important for the maintenance of this cell. In the Tyrrhenian Sea, the residual overturning circulation mainly flows along isopycnals, thus indicating a more adiabatic balance.

However, the main differences between Eulerian and residual zonal overturning appear in the EMED. The residual circulation is weaker at depth than the Eulerian circulation, and a detectable residual counterclockwise circulation emerges. The large and deep Eulerian clockwise cell is broken into two parts in the residual representation: the deep overturning at 22° E is along isopycnals, while the circulation around the secondary maxima located approximately in the Rhodes gyre area of 28° E is across-isopycnals. The deep to abyssal ZOC of the EMED is strongly influenced by the transport due to the eddy/permanent gyres component. This analysis covers the period of the EMT event, and the Aegean deep water source is apparent in the zonal overturning cell of the Mediterranean Sea.

7.6.2 Western Mediterranean overturning

The Mediterranean has multiple subbasins and an opening at the Gibraltar Strait, and thus its geometry does not easily fit the traditional zonal integration associated with meridional overturning circulation.

Integrating over a subsection of longitudes is thus more informative, as it separates the meridional overturning of the WMED and the EMED. Again, the overturning

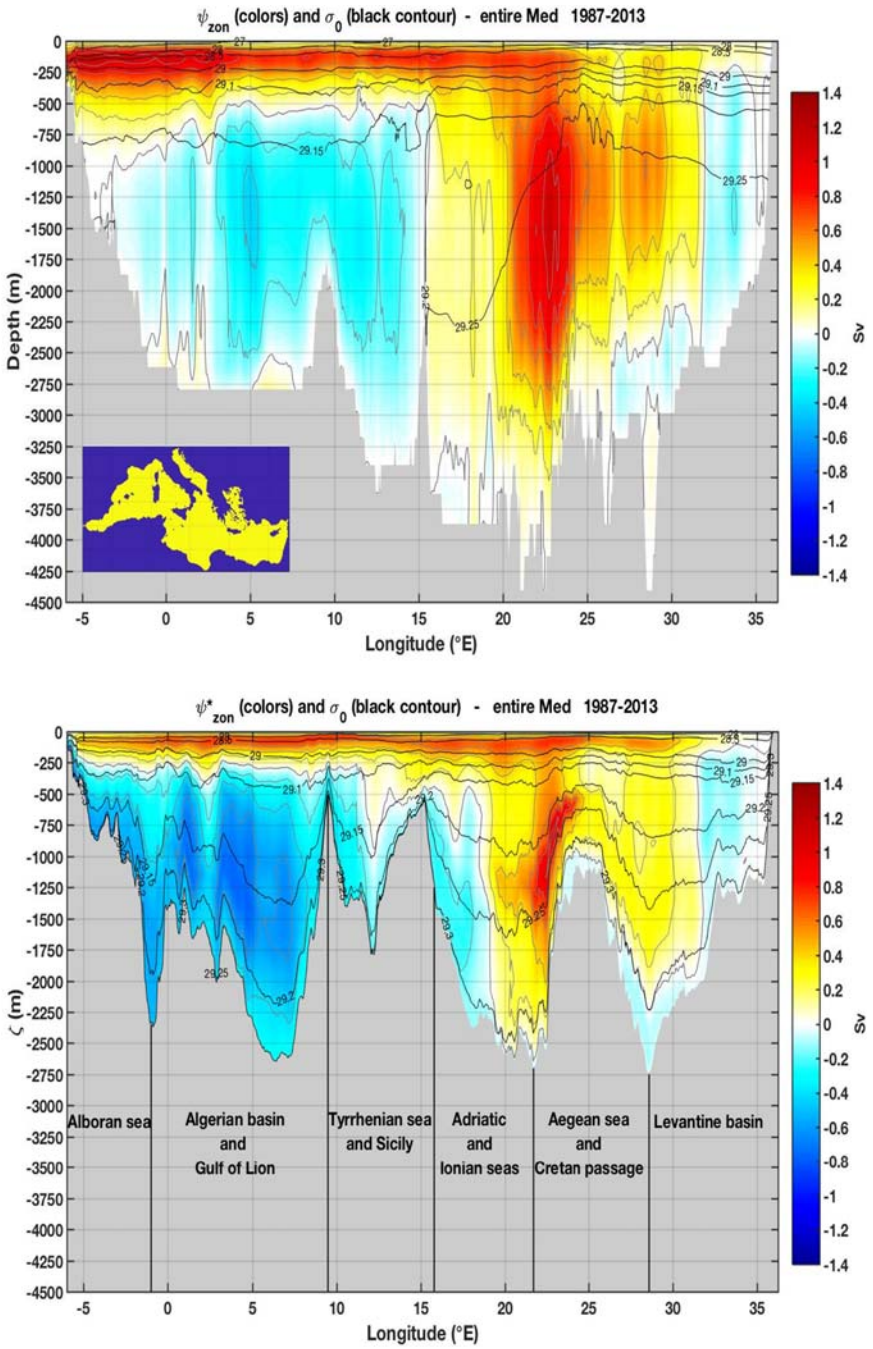
ψzon (colors) and σ0 (black contour) - entire Med 1987-2013
Depth (m)
Longitude (°E)
Sv
ψ*zon (colors) and σ0 (black contour) - entire Med 1987-2013
ζ (m)
Alboran sea
Algerian basin and Gulf of Lion
Tyrrhenian sea and Sicily
Adriatic and Ionian seas
Aegean sea and Cretan passage
Levantine basin
Longitude (°E)
Sv

FIGURE 7.16

streamfunction is shown with either depth (Eulerian streamfunction) or density (residual streamfunction) as a vertical coordinate, and with latitude as the horizontal coordinate.

The Eulerian streamfunction (Fig. 7.17, top panel) consists of a clockwise cell with multiple maxima from 100 m down to 2000 m. Counterclockwise cells, with maximum transport in the deep Algerian basin, occupy the abyssal Mediterranean region (the large positive values are above 500 m, just south of 37° N, and are associated with the Gibraltar Strait inflow). The residual WMED (bottom panel) meridional overturning shows only two well-separated counter-rotating cells, which are both stronger than their Eulerian counterparts. The clockwise streamfunction has a maximum volume transport of approximately 0.36 Sv, while the residual streamfunction reaches 0.88 Sv. For the counterclockwise cells, the minimum of −0.22 Sv in the Eulerian framework increases to −0.7 Sv in the residual streamfunction. The strengthening of the residual flow compared to the Eulerian flow is consistent with the WMED spreading of deep water being dominated by eddies, and their transport is only captured by the integration in the density coordinates. The boundary between the two residual cells is at approximately 39° N, i.e., the latitude marking the division between the permanent cyclonic gyre of the Gulf of Lion and the eddy-dominated anticyclonic area of the Algerian current, as described by Pinardi et al. (2015) and Demirov and Pinardi (2007). The clockwise northern cell is associated with the DWF areas in the northern basin, which are typically centered around 41−42° N.

7.6.3 Eastern Mediterranean overturning

Capturing the DWF areas in marginal seas such as the Adriatic and the Aegean allows to resolve the meridional overturning of the EMED. The Eulerian overturning (Fig. 7.18, top panel) is complex, with a shallow clockwise circulation in the Adriatic, Ionian, and Aegean Seas associated with the respective DWFs (Verri et al., 2018). This deepens south of the Rhodes gyre and Levantine Seas areas and is associated with their respective DWFs processes (Velaoras et al., 2014). The near-surface anticlockwise cell south of the Sicily Channel is associated with the Ekman transport and its shallow return flow. The deep counterclockwise Eulerian cell below 1000 m

Eulerian (top) and residual (bottom) zonal streamfunction, integrated over the latitudinal extension of the basin and averaged in time from 1987 to 2013. The gray contour lines and the colors show values at 0.2 Sv intervals. The black contours are isopycnal surfaces of σ (in kg m^{-3}) latitudinally and time averaged (top), calculated as described in Pinardi et al. (2019) (bottom). The gray areas mark the deepest bathymetry level (top) and the highest density layer depth (bottom) found over each latitudinal section of the basin. The different regions of the Mediterranean considered in the latitudinal averaging are described on the gray area of the bottom panel.

From Pinardi, N., Cessi, P., Borile, F., Wolfe, C.L., 2019. The Mediterranean Sea overturning circulation. J. Phys. Oceanogr. 49 (7), 1699–1721.

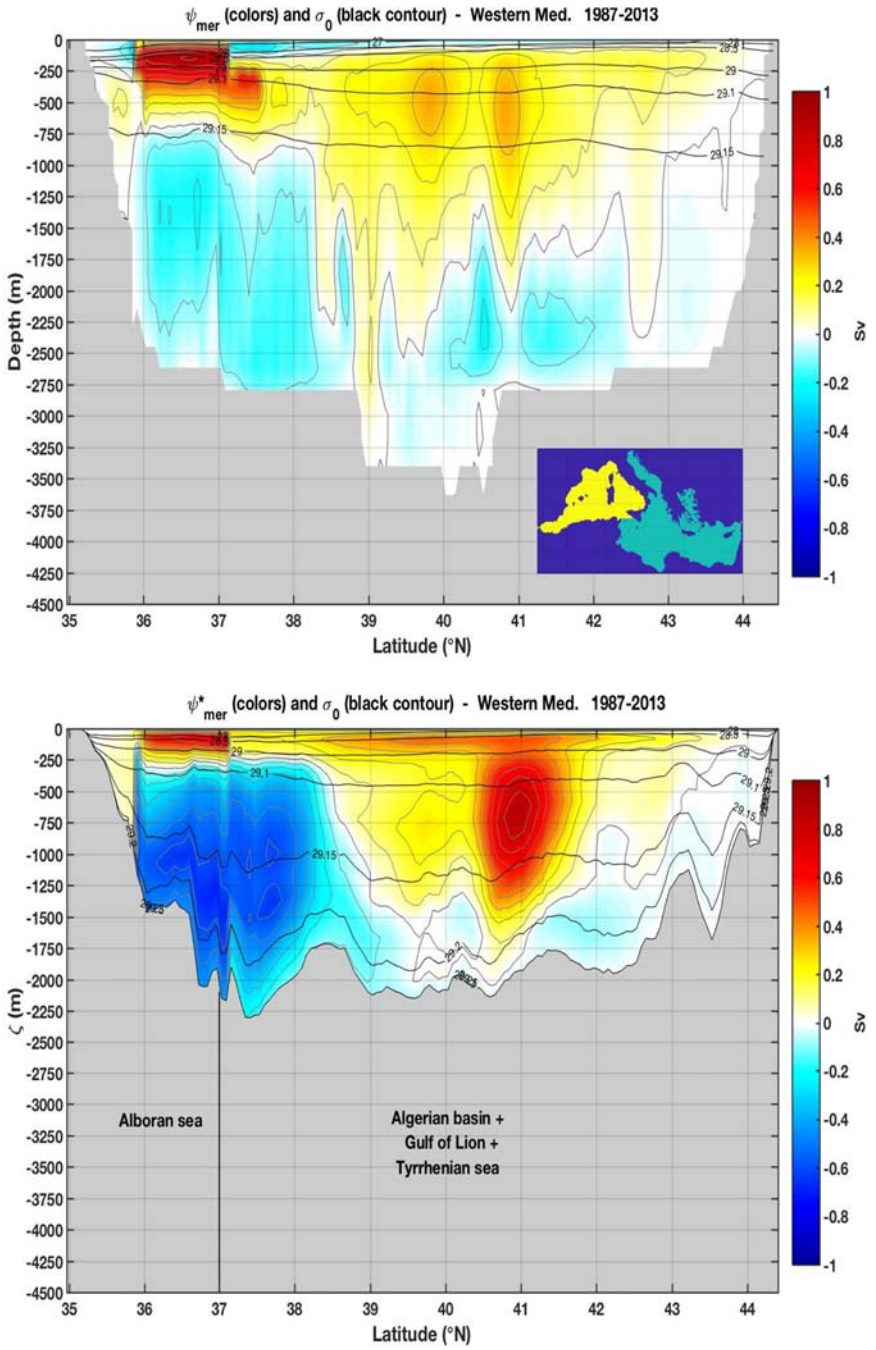
ψ_{mer} (colors) and σ_0 (black contour) - Western Med. 1987-2013
Depth (m)
Latitude (°N)
Sv
ψ^*_{mer} (colors) and σ_0 (black contour) - Western Med. 1987-2013
ζ (m)
Alboran sea
Algerian basin +
Gulf of Lion +
Tyrrhenian sea
Latitude (°N)
Sv

FIGURE 7.17

has been previously described (Zavatarelli and Mellor, 1995; Pisacane et al., 2006; Verri et al., 2018). The deep counterclockwise circulation is reduced in the residual framework (Fig. 7.18, bottom panel), while the clockwise circulation is enhanced relative to the Eulerian measure. The southern maximum of the clockwise residual cell corresponds to the region of dense Aegean Sea water outflows and the Rhodes gyre southern areas.

7.6.4 Comparison of the Mediterranean with the North Atlantic overturning

The Mediterranean Sea has been referred to as a miniature ocean in climate studies (Bethoux et al., 1999; Tsimplis et al., 2006) because it is a basin with deep and intermediate water mass formation processes that generate a vigorous overturning circulation. In this section, the similarities and differences between the Atlantic meridional overturning circulation (AMOC), the global overturning circulation (GOC) and the Mediterranean overturning are discussed.

The AMOC and GOC are primarily visualized in terms of meridional cells. The Atlantic sector is dominated by an interhemispherical clockwise mid-depth cell (Fig. 7.19, top panel), i.e., the AMOC, with downwelling in the high latitudes of the North Atlantic and upwelling in the global ocean. The GOC is characterized by the clockwise mid-depth circulation associated with the AMOC and an abyssal clockwise cell with downwelling in the high latitudes of the southern hemisphere. Most of the abyssal cell occurs in the Indo-Pacific sector (Fig. 7.19, bottom panel). The longitudinal integration gives the impression that the mid-depth and abyssal cells are separated, but these 2 cells are interconnected in three dimensions. A proportion of the water in the lower branch of the AMOC circulates in the abyssal cell before rejoining the upper branch of the AMOC, and becomes denser before it upwells. Estimates of this proportion range from 50% to 100% (Lumpkin and Speer, 2007; Talley, 2013; Rousselet et al., 2021). The mid-depth cell primarily "feeds" the abyssal cell in the Weddell Sea gyre and at the Campbell Plateau-Chatham Rise, just east of New Zealand, where the deep western boundary current of the South Pacific enters the abyssal Pacific basin.

Eulerian (top) and residual (bottom) meridional streamfunctions for the WMED, integrated in longitude over the yellow region shown in the inset and averaged in time over the years 1987–2013. The gray contour lines and the colors show values at 0.1 Sv intervals. The black contours are isopycnal surfaces of σ (in kg m^{-3}) longitudinally and time averaged (top), calculated as described in Pinardi et al. (2019) (bottom). The gray areas mark the deepest bathymetry level (top) and the highest density layer depth (bottom) found over each longitudinal section of the basin. The different regions of the Mediterranean considered in the longitudinal averaging are described over the gray area of the bottom panel.

From Pinardi, N., Cessi, P., Borile, F., Wolfe, C.L., 2019. The Mediterranean Sea overturning circulation. J. Phys. Oceanogr. 49 (7), 1699–1721.

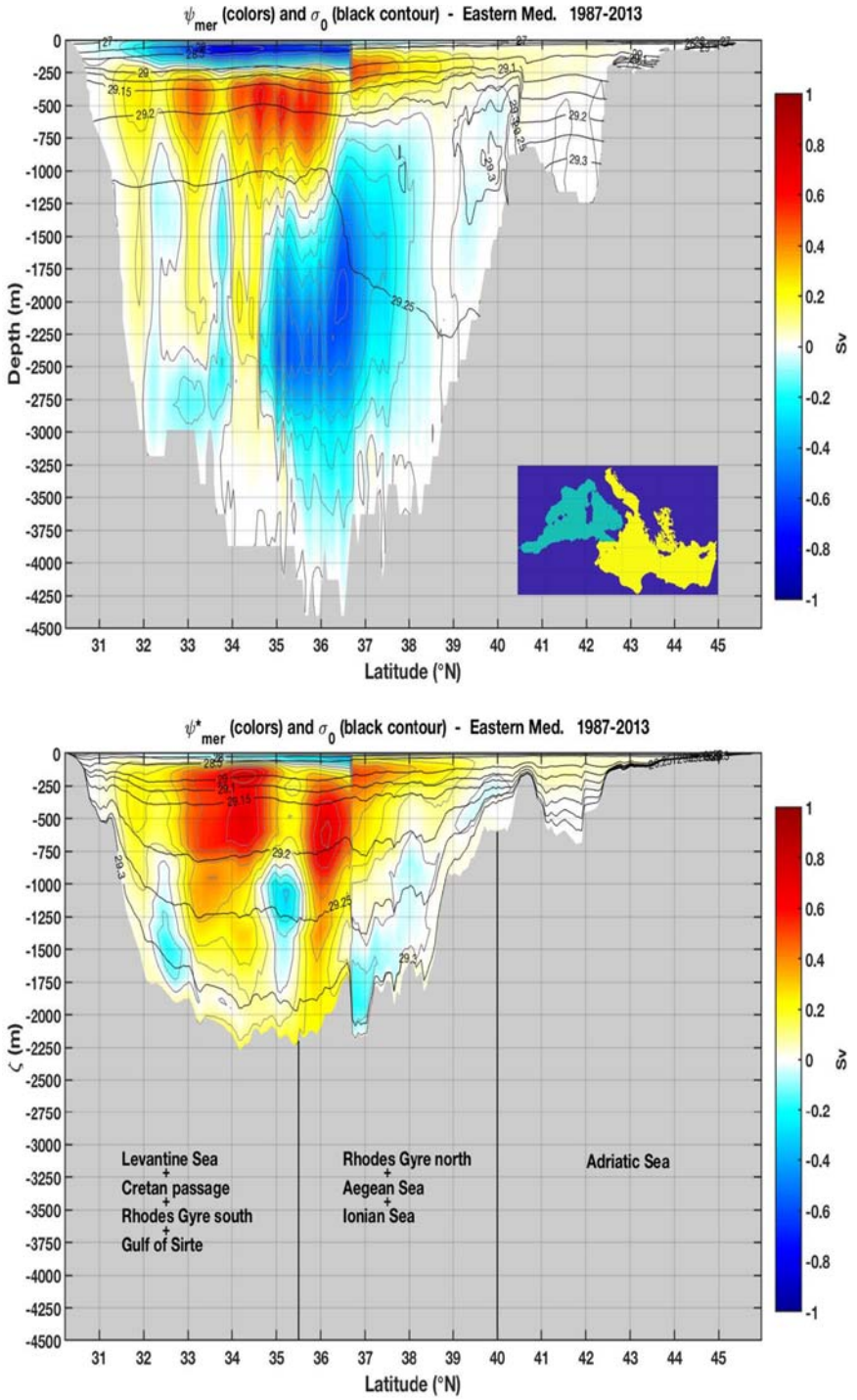
ψmer (colors) and σ0 (black contour) - Eastern Med. 1987-2013
Depth (m)
Latitude (°N)
Sv
ψ*mer (colors) and σ0 (black contour) - Eastern Med. 1987-2013
ζ (m)
Levantine Sea
+
Cretan passage
+
Rhodes Gyre south
+
Gulf of Sirte
Rhodes Gyre north
+
Aegean Sea
+
Ionian Sea
Adriatic Sea
Latitude (°N)
Sv

FIGURE 7.18

Eulerian (top) and residual (bottom) meridional streamfunctions of the EMED, integrated in longitude over the yellow region shown in the inset and averaged in time over the years 1987–2013. The gray contour lines and the colors show values at 0.1 Sv intervals. The black contours are isopycnal surfaces of σ (in kg m^{-3}) longitudinally and time averaged (top), calculated as described in Pinardi et al. (2019) (bottom). The gray areas mark the deepest bathymetry level (top) and the highest density layer depth (bottom) found over each longitudinal section of the basin. The different regions of the Mediterranean considered in the longitudinal averaging are described over the gray area of the bottom panel.

FromPinardi, N., Cessi, P., Borile, F., Wolfe, C.L., 2019. The Mediterranean Sea overturning circulation. J. Phys. Oceanogr. 49 (7), 1699–1721.

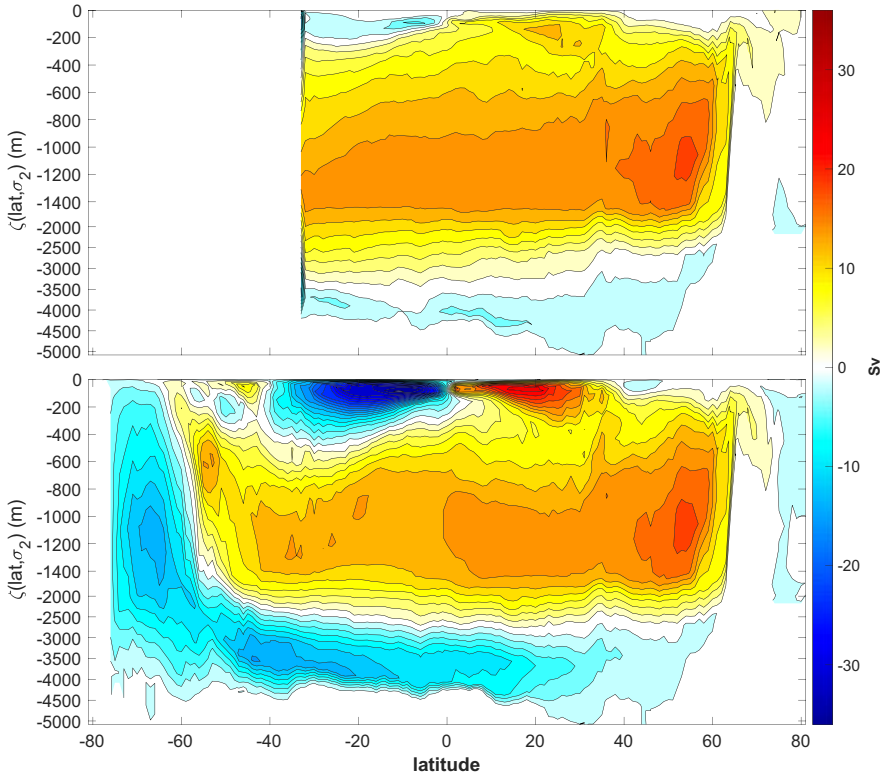

FIGURE 7.19

Residual meridional streamfunction integrated over the Atlantic sector north of 33° S (top) and the global ocean (bottom), and averaged in time over the years 1992–2015, using the Estimating the Circulation and Climate of the Ocean (ECCO) assimilated model. The black contour lines and the colors show values at 2 Sv intervals.

The mid-depth AMOC is powered by the winds of the Antarctic circumpolar region and is enabled by surface high density in the high latitudes of the North Atlantic (Toggweiler and Samuels, 1993). The AMOC mainly flows along isopycnals, except at the endpoints where strong diapycnal upwelling and downwelling occurs (Wolfe and Cessi, 2011). In contrast, the abyssal circulation is powered by diapycnal upwelling associated with the breaking of internal gravity waves near rough topography and balances the near-surface negative buoyancy flux in the downwelling regions, primarily in the Southern Ocean.

The Mediterranean ZOC or Wüst cell can be regarded as analogous to the mid-depth AMOC, although the ZOC is visualized as a zonal circulation and the AMOC as a meridional circulation. In Fig. 7.18 the mean pathways of the zonal and meridional vertical circulation are shown: between the surface and 150 m for the AW; between 150 and 1000 m for LIW/CIW; and below 1000 m for deep waters. The upper branch of the ZOC enters from Gibraltar and feeds the intermediate and deep waters following a two-step process. It is first converted into intermediate waters in the Eastern Levantine basin and then to deep waters in the four open ocean DWF areas 1,2, 4 and 8 (Fig. 7.3).

The zonal predominance of the Wüst cell is not only due to the geometrical differences between the Mediterranean and the Atlantic, but also to its energy source. The ZOC is powered by the inflow/outflow at the Gibraltar Strait, which in turn is balanced by the wind-stress work and the buoyancy flux in the basin (Cessi et al., 2014). Thus, the Mediterranean ZOC is locally powered, while the AMOC is powered remotely by wind-stress outside the Atlantic basin. Both the AMOC and the Mediterranean ZOC mainly flow along isopycnals, indicating that mixing is not the main driver of these cells.

Similarly, the deep clockwise circulation in the WMED can be viewed as analogous to the anticlockwise global abyssal circulation (which is primarily confined to the southern hemisphere). Both these cells are primarily driven by diapycnal mixing and reach the deepest part of the basins they flow into.

Similar to the feeding of the abyssal cell of the GOC by the AMOC, the Wüst cell return flow (150−1000°m) is an essential component of the WMED and EMED deep overturning. In Fig. 7.20 this effect is illustrated through the contribution of the LIW to DWF in the four areas of the Aegean, the Adriatic and the Gulf of Lion. The inflowing LIW in these areas increases the salinity of the local intermediate waters and preconditions the deep convection of the EMED and WMED cells. Another path flows directly to the Gibraltar Strait, providing a direct closure of the lower branch of the Wüst cell. The densification of LIW as it enters the abyssal waters of the Mediterranean before exiting at the Gibraltar Strait (at a shallower and lighter level than the abyss) is analogous to the interconnection between the mid-depth and abyssal cells in the global ocean.

Modern computations with and without assimilated data also indicate LIW eddy-dominated transport connecting the western Sardinia to the Balearic slopes, which merges with the LIW flowing from the Gulf of Lion (Pinardi et al., 2019; Estournel et al., 2021). However, this path is not depicted in Fig. 7.20 as its relative transport

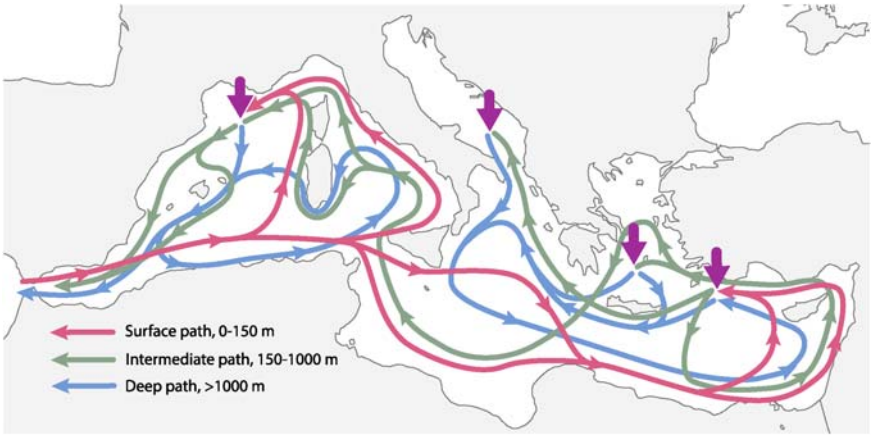

FIGURE 7.20

The vertical pathways at three different depths. The surface to upper ocean circulation is denoted by the red ribbon, the intermediate to deep is green and the abyssal circulation blue. DWF occurs where one color joins a different color and the four locations are denoted by downward purple arrows. Shelf DWF and cascading is not considered.

with respect to the other paths over multidecadal time scales is not yet clear. Similarly, the surface path from the Malta shelf escarpment toward the Adriatic Sea is also omitted as it was part of the EMT and it is not a persistent feature (Malanotte-Rizzoli et al., 1997).

In a recent work, Amitai et al. (2021) shows that the two deep water sources of the EMED, the Adriatic and the Aegean Seas, largely influence the WMED intermediate water pathways and finally the DWF occurring in the Gulf of Lion. If the Adriatic Sea source is depressed (as shown in Fig. 7.4 during the EMT), smaller volumes of deep waters are exchanged at the Sicily Channel. Furthermore, when the Adriatic is depressed, the intermediate and deep waters coming from the Sicily Channel reach the Gulf of Lion region more frequently. On the contrary, when the Adriatic is active, the water flowing along the eastern Tyrrhenian is diluted with deep Tyrrhenian water; hence, less water mass trajectories arrive to the Gulf of Lion area.

The abyssal pathways for the EMED were simulated by (Curchitser et al., 2001) and those of the WMED by Send and Testor (2017) with average drifting float trajectories. In both basins, the abyssal circulation is cyclonic and is connected to the four open ocean deep water sources previously described.

7.7 Concluding remarks

This chapter reviewed the observational, theoretical and numerical scientific studies of the past 50 years that examined the complex DWF and redistribution processes occurring in the Mediterranean Sea.

Several DWF areas have been detected and at least nine areas of DWF have been identified, with four of them involving open ocean DWF processes. These pervasive dense water transformation processes occur at submesoscales and on the shelf, with bathymetric-specific structures and with the semienclosed nature of DWF subbasins having significant effects (Aegean and Adriatic Seas). The interannual variability of formation rates is now well-established for both the EMED and the WMED, with 3–5 year-long periods in which formation rates are high, intertwined with low formation rate periods of equivalent length. The EMT (see Chapter 9) is a key dense/deep water event of the past 30 years and has affected the vertical circulation of the basin.

The Mediterranean Sea vertical circulation is vigorous both in the EMED and WMED. The Gibraltar Strait inflow waters are converted into intermediate waters, forming the ZOC of the basin: its lower branch is composed of LIW/CIW, which partially become denser in the open ocean DWF areas before exiting through the Gibraltar Strait into the Atlantic. The meridional overturning is different in the Eulerian and Lagrangian frameworks, indicating the importance of eddy transport and diabatic mixing processes. Lyubartsev et al. (2020) devises an index that shows the interannual variability of the WMED and EMED meridional clockwise cells: the preliminary findings show that in a 32 year period (1987–2018), the EMED has larger index values than the WMED indicating larger vertical transports. Furthermore, the index maxima coincide with the EMT and the 2004–05 WMDW formation events.

A significant connection between intermediate depth and the meridional component of the vertical circulation is likely similar to the situation in the global ocean between the AMOC and the abyssal circulation of the global ocean. A schematic of the surface, intermediate, and abyssal circulations of the Mediterranean Sea demonstrates the interconnections between the zonal and meridional overturning cells.

Much remains to be understood, including the eddy-driven intermittent transport of waters in various basin subportions, the effective contribution of the shelf DWF mechanisms in the meridional circulation, the long-term trends due to climate and hydrological changes, and the links between the Atlantic and Mediterranean Seas.

Additional resources

- CMEMS, https://marine.copernicus.eu/

References

Adani, M., Dobricic, S., Pinardi, N., 2011. Quality assessment of a 1985–2007 Mediterranean Sea reanalysis. J. Atmos. Ocean. Technol. 28 (4), 569–589.

Allen, J.T., Painter, S.C., Rixen, M., 2008. Eddy transport of western Mediterranean intermediate water to the Alboran Sea. J. Geophys. Res. C Oceans Atmos. 113, C04024.

Amitai, Y., Ashkenazy, Y., Gildor, H., 2021. The effect of the source of deep water in the eastern Mediterranean on western Mediterranean intermediate and deep water. Front. Mar. Sci. 7, 615975.

Anati, D., Stommel, H., 1970. The initial phase of deep water formation in the northwest Mediterranean, during MEDOC69, on the basis of observations made by Atlantic II, January 25−February 12, 1969. Cah. Oceanogr. XXII (4), 343−351.

Anati, D.A., 1971. On the mechanism of the deep mixed layer formation during Medoc 69. Cah. Oceanogr. 23 (4), 427−443.

Artale, V., Astraldi, M., Buffoni, G., Gasparini, G., 1994. Seasonal variability of gyre-scale circulation in the northern Tyrrhenian Sea. J. Geophys. Res. 991, 14127−14138.

Artegiani, A., Bregant, D., Paschini, E., Pinardi, N., Raicich, F., Russo, A., 1997. The Adriatic Sea General Circulation. Part I: air-sea interactions and water mass structure. J. Phys. Oceanogr. 27, 1492−1514.

Ben Ismail, S., Schroeder, K., Sammari, C., Gasparini, G.P., Borghini, M., Aleya, L., 2014. Interannual variability of water mass properties in the Tunisia−Sicily Channel. J. Mar. Syst. 135, 14−28.

Bensi, M., Cardin, V., Rubino, A., Notarstefano, G., Poulain, P.M., 2013. Effects of winter convection on the deep layer of the Southern Adriatic Sea in 2012. J. Geophys. Res. Oceans 118, 6064−6075.

Bethoux, J.P., Gentili, B., Morin, P., Nicolas, E., Pierre, C., Ruiz-Pino, D., 1999. The Mediterranean Sea: a miniature ocean for climatic and environmental studies and a key for the climatic functioning of the North Atlantic. Prog. Oceanogr. 44 (1−3), 131−146.

Beuvier, J., Béranger, K., Lebeaupin Brossier, C., Somot, S., Sevault, F., Drillet, Y., Bourdallé-Badie, R., Ferry, N., Lyard, F., 2012. Spreading of the western Mediterranean deep water after winter 2005: time scales and deep cyclone transport. J. Geophys. Res. 117, C07022.

Bosse, A., Testor, P., Houpert, L., Damien, P., Prieur, L., Hayes, D., Taillandier, V., Durrieu de Madron, X., d'Ortenzio, F., Coppola, L., Karstensen, J., Mortier, L., 2016. Scales and dynamics of submesoscale coherent vortices formed by deep convection in the northwestern Mediterranean Sea. J. Geophys. Res. Oceans 121, 7716−7742.

Bosse, A., Testor, P., Damien, P., Estournel, C., Marsaleix, P., Mortier, L., Prieur, L., Taillandier, V., 2021. Wind-forced submesoscale symmetric instability around deep convection in the northwestern Mediterranean Sea. Fluid 6 (3), 123.

Boyer, T.P., Baranova, O.K., Coleman, C., Garcia, H.E., Grodsky, A., Locarnini, R.A., Mishonov, A.V., Paver, C.R., Reagan, J.R., Seidov, D., Smolyar, I.V., Weathers, K., Zweng, M.M., 2018. World ocean database 2018. In: Mishonov, A.V., Technical (Eds.), NOAA Atlas NESDIS, vol. 87.

Canals, M., Puig, P., Durrieu de Madron, X., Heussner, S., Palanques, A., Fabres, J., 2006. Flushing submarine canyons. Nature 444, 354−357.

Castellari, S., Pinardi, N., Leaman, K., 1998. A model study of air-sea interactions in the Mediterranean Sea. J. Mar. Syst. 18, 89−114.

Castellari, S., Pinardi, N., Leaman, K., 2000. Simulation of water mass formation processes in the Mediterranean Sea: influence of the time frequency of the atmospheric forcing. J. Geophys. Res. 105 (C10), 24157−24181.

Cessi, P., Pinardi, N., Lyubartsev, V., 2014. Energetics of semienclosed basins with two-layer flows at the Strait. J. Phys. Oceanogr. 44, 967−979.

Curchitser, E.N., Haidvogel, D.B., Iskandarani, M., 2001. Transient adjustment of circulation in a midlatitude abyssal ocean basin with realistic geometry and bathymetry. J. Phys. Oceanogr. 31 (3), 725−745.

Cushman-Roisin, B., Poulain, P.M., Gacic, M., Artegiani, A., 2001. Physical Oceanography of the Adriatic Sea. Springer, Dordrecht. https://doi.org/10.1007/978-94-015-9819-4.

Damien, P., Bosse, A., Testor, P., Marsaleix, P., Estournel, C., 2017. Modeling postconvective submesoscale coherent vortices in the northwestern Mediterranean Sea. J. Geophys. Res. Oceans 122, 9937−9961.

Demirov, E., Pinardi, N., 2002. The Simulation of the Mediterranean Sea circulation from 1979 to 1993. Part I: the interannual variability. J. Mar. Syst. 33−34, 23−50.

Demirov, E.K., Pinardi, N., 2007. On the relationship between the water mass pathways and eddy variability in the Western Mediterranean Sea. J. Geophys. Res. 112, C02024.

Dewar, W.K., Killworth, P.D., 1990. On the cylinder collapse problem, mixing, and the merger of isolated eddies. J. Phys. Oceanogr. 20, 1563−1575.

Dufau-Julliand, C., Marsaleix, P., Petrenko, A., Dekeyser, I., 2004. Three-dimensional modeling of the Gulf of Lion's hydrodynamics (northwest Mediterranean) during January 1999 (MOOGLI3 Experiment) and late winter 1999: western Mediterranean Intermediate Water's (WIW's) formation and its cascading over the shelf break. J. Geophys. Res. 109, C11002.

Durrieu de Madron, X., Houpert, L., Puig, P., Sanchez-Vidal, A., Testor, P., Bosse, A., Estournel, C., Somot, S., Bourrin, F., Bouin, M.N., Beauverger, M., Beguery, L., Calafat, A., Canals, M., Cassou, C., Coppola, L., Dausse, D., D'Ortenzio, F., Font, J., Heussner, S., Kunesch, S., Lefevre, D., Le Goff, H., Martín, J., Mortier, L., Palanques, A., Raimbault, P., 2013. Interaction of dense shelf water cascading and open-sea convection in the northwestern Mediterranean during winter 2012. Geophys. Res. Lett. 40, 1379−1385.

Escudier, R., Clementi, E., Cipollone, A., Pistoia, J., Drudi, M., Grandi, A., Lyubartsev, V., Lecci, R., Aydogdu, A., Delrosso, D., Omar, M., Masina, S., Coppini, G., Pinardi, N., 2021. A high resolution reanalysis for the Mediterranean Sea. Front. Earth Sci. 9, 702285.

Estournel, C., Testor, P., Taupier-Letage, I., Bouin, M.-N., Coppola, L., Durand, P., Conan, P., Bosse, A., Brilouet, P.-E., Beguery, L., Belamari, S., Béranger, K., Beuvier, J., Bourras, D., Canut, G., Doerenbecher, A., Durrieu de Madron, X., D'Ortenzio, F., Drobinski, P., Ducrocq, V., Fourrié, N., Giordani, H., Houpert, L., Labatut, L., Brossier, C.L., Nuret, M., Prieur, L., Roussot, O., Seyfried, L., Somot, S., 2016a. HyMeX-SOP2: the field campaign dedicated to dense water formation in the northwestern Mediterranean. Oceanography 29 (4), 196−206.

Estournel, C., Testor, P., Damien, P., D'Ortenzio, F., Marsaleix, P., Conan, P., Kessouri, F., Durrieu de Madron, X., Coppola, L., Lellouche, J.M., Belamari, S., Mortier, L., Ulses, C., Bouin, M.N., Prieur, L., 2016b. High resolution modeling of dense water formation in the north-western Mediterranean during winter 2012−2013: processes and budget. J. Geophys. Res. Oceans 121, 5367−5392.

Estournel, C., Marsaleix, P., Ulses, C., 2021. A new assessment of the circulation of Atlantic and intermediate waters in the eastern Mediterranean. Prog. Oceanogr. 198, 102673.

Fuda, J.L., Millot, C., Taupier-Letage, I., Send, U., Bocognano, J.M., 2000. XBT monitoring of a meridian section across the western Mediterranean Sea. Deep-Sea Res. I 47, 2191−2218.

Fuda, J.-L., Etiope, G., Millot, C., Favali, P., Calcara, M., Smriglio, G., Boschi, E., 2002. Warming, salting and origin of the Tyrrhenian deep water. Geophys. Res. Lett. 29 (19), 1898.

Gačić, M., Lascaratos, A., Manca, B.B., Mantziafou, A., 2001. Adriatic deep water and interaction with the eastern Mediterranean Sea. In: Cushman-Roisin, B., Gačić, M.,

Poulain, P.M., Artegiani, A. (Eds.), Physical Oceanography of the Adriatic Sea. Springer, Dordrecht.
Gascard, J.C., 1973. Vertical motions in a region of deep water formation. Deep-Sea Res. Oceanogr. Abstr. 20 (11), 1011−1027.
Gascard, J.C., 1978. Mediterranean deep-water formation baroclinic instability and oceanic eddies. Oceanol. Acta 1 (3), 315−330.
Gascard, J.-C., Richez, C., 1985. Water masses and circulation in the western Alboran Sea and in the Straits of Gibraltar. Prog. Oceanogr. 15, 157−216.
Gasparini, G.P., Zodiatis, G., Astraldi, M., Galli, C., Sparnocchia, S., 1999. Winter intermediate water lenses in the Ligurian Sea. J. Mar. Syst. 20, 319−332.
Gertman, I.F., Ovchinnikov, I.M., Popov, Y.I., 1994. Deep convection in the eastern basin of the Mediterranean Sea. Oceanology 34 (1), 19−25.
Gertman, I., Pinardi, N., Popov, Y., Hecht, A., 2006. Aegean Sea water masses during the early stages of the eastern Mediterranean climatic transient (1988−1990). J. Phys. Oceanogr. 36 (9), 1841−1859.
Hecht, A., Pinardi, N., Robinson, A., 1988. Currents, water masses, eddies and jets in the Mediterranean Levantine Basin. J. Phys. Oceanogr. 18, 1320−1353.
Iovino, D., Straneo, F., Spall, M., 2008. On the effect of a sill on dense water formation in a marginal sea. J. Mar. Res. 66 (3), 325−345.
Ivanov, V.V., Shapiro, G.I., Huthnance, J.M., Aleynik, D.L., Golovin, P.N., 2004. Cascades of dense water around the world ocean. Prog. Oceanogr. 60, 47−98.
Jones, H., Marshall, J., 1993. Convection with rotation in a neutral ocean: a study of open-ocean deep convection. J. Phys. Oceanogr. 23 (6), 1009−1039.
Josey, S.A., 2003. Changes in the heat and freshwater forcing of the eastern Mediterranean and their influence on deep water formation. J. Geophys. Res. 108 (C7), 3237.
Juza, M., Escudier, R., Vargas-Yáñez, M., Mourre, B., Heslop, E., Allen, J., Tintoré, J., 2019. Characterization of changes in Western Intermediate Water properties enabled by an innovative geometry-based detection approach. J. Mar. Syst. 191, 1−12.
Killworth, P.D., 1976. The mixing and spreading phases of MEDOC.I. Prog. Oceanogr. 7 (2), 59−90.
Kokkini, Z., Mauri, E., Gerin, R., Poulain, P.M., Simoncelli, S., Notarstefano, G., 2020. On the salinity structure in the South Adriatic as derived from float and glider observations in 2013−2016. Deep-Sea Res. Part II 171, 104625.
Lascaratos, A., 1993. Estimation of deep and intermediate water mass formation rates in the Mediterranean Sea. Deep-Sea Research II 40 (6), 1327−1333.
Lascaratos, A., Roether, W., Nittis, K., Klein, B., 1999. Recent changes in deep water formation and spreading in the eastern Mediterranean Sea: a review. Prog. Oceanogr. 44, 5−36.
Leaman, K.D., Schott, F.A., 1991. Hydrographic structure of the convection regime in the Gulf of Lions: winter 1987. J. Phys. Oceanogr. 21 (4), 575−598.
Legg, S., Marshall, J., 1993. A heton model of the spreading phase of open-ocean deep convection. J. Phys. Oceanogr. 23 (6), 1040−1056.
LIWEX Group, 2003. The Levantine Intermediate Water Experiment (LIWEX) Group: Levantine basin—a laboratory for multiple water mass formation processes. J. Geophys. Res. 108, 8101.
López-Jurado, J., Lafuente, J.M.G., Lucaya, N.C., 1995. Hydrographic conditions of the Ibiza Channel during November 1990, March 1991 and July 1992. Oceanol. Acta 18 (2), 235−243.

Lumpkin, R., Speer, K., 2007. Global ocean meridional overturning. J. Phys. Oceanogr. 37 (10), 2550−2562.

Lyubartsev, V., Borile, F., Clementi, E., Masina, S., Drudi, M., Coppini, G., Cessi, P., Pinardi, N., 2020. Interannual variability in the eastern and western Mediterranean overturning index. Copernicus marine service ocean state report, issue 4. J. Oper. Oceanogr. 13, S1−S172.

Madec, G., Delecluse, P., Crepon, M., Chartier, M., 1991. A three-dimensional numerical study of deep-water formation in the northwestern Mediterranean Sea. J. Phys. Oceanogr. 21 (9), 1349−1371.

Madec, G., Delecluse, P., Crépon, M., Lott, F., 1996. Large-scale preconditioning of deep-water formation in the northwestern Mediterranean Sea. J. Phys. Oceanogr. 26 (8), 1393−1408.

Malanotte-Rizzoli, P., Robinson, A.R., 1994. Ocean processes in climate dynamics: global and Mediterranean examples. In: Proceedings of NATO-ASI. Kluwer Academic Publishers, Dordrecht, The Netherlands, p. 437.

Malanotte-Rizzoli, P., Manca, B.B., Ribera D'Alcalà, M., Theocharis, A., Bergamasco, A., Bregant, D., Budillon, G., Civitarese, G., Georgopoulos, D., Michelato, A., Sansone, E., Scarazzato, P., Souvermezoglou, E., 1997. A synthesis of the Ionian Sea hydrography, circulation and water mass pathways during POEM-Phase I. Prog. Oceanogr. 39 (3), 153−204.

Manca, B.B., Budillon, G., Scarazzato, P., Ursella, L., 2003. Evolution of dynamics in the eastern Mediterranean affecting water mass structures and properties in the Ionian and Adriatic Seas (1995−1999). J. Geophys. Res. Oceans 108, C9.

Manca, B.B., Ibello, V., Pacciaroni, M., Scarazzato, P., Giorgetti, A., 2006. Ventilation of deep waters in the Adriatic and Ionian Seas following changes in thermohaline circulation of the Eastern Mediterranean. Clim. Res. 31, 239−256.

Mantziafou, A., Lascaratos, A., 2004. An eddy resolving numerical study of the general circulation and deep-water formation in the Adriatic Sea. Deep Sea Res. Oceanogr. Res. Pap. 51, 921−952.

Margirier, F., Bosse, A., Testor, P., L'Heveder, B., Mortier, L., Smeed, D., 2017. Characterization of convective plumes associated with oceanic deep convection in the northwestern Mediterranean from high-resolution in situ data collected by gliders. J. Geophys. Res. Oceans 122, 9814−9826.

Margirier, F., Testor, P., Heslop, E., Mallil, K., Bosse, A., Houpert, L., Mortier, L., Bouin, M.N., Coppola, L., D'Ortenzio, F., Durrieu de Madron, X., Mourre, B., Prieur, L., Raimbault, P., Taillandier, V., 2020. Abrupt warming and salinification of intermediate waters interplays with decline of deep convection in the Northwestern Mediterranean Sea. Sci. Rep. 10, 20923.

Marini, M., Grilli, F., Guarnieri, A., Jones, B.H., Klajic, Z., Pinardi, N., Sanxhaku, M., 2010. Is the southeastern Adriatic Sea coastal strip an eutrophic area? Estuar. Coast Shelf Sci. 88, 395−406.

Marshall, J., Schott, F., 1999. Open-ocean convection: observations, theory, and models. Rev. Geophys. 37 (1), 1−64.

Maxworthy, T., Narimousa, S., 1994. Unsteady, turbulent convection into a homogeneous, rotating fluid, with oceanographic applications. J. Phys. Oceanogr. 24 (5), 865−887.

McWilliams, J.C., 1985. Submesoscale, coherent vortices in the ocean. Rev. Geophys. 23 (2), 165−182.

MEDOC Group, 1970. Observation of formation of deep water in the Mediterranean Sea, 1969. Nature 227.

Mihanović, H., Vilibić, I., Carniel, S., Tudor, M., Russo, A., Bergamasco, A., Bubić, N., Ljubešić, Z., Viličić, D., Boldrin, A., Malačič, V., Celio, M., Comici, C., Raicich, F., 2013. Exceptional dense water formation on the Adriatic shelf in the winter of 2012. Ocean Sci. 9, 561−572.

Millot, C., 1987. Circulation in the western Mediterranean Sea. Oceanol. Acta 10 (2), 143−149.

Millot, C., 1999. Circulation in the western Mediterranean Sea. J. Mar. Syst. 20, 423−442.

Millot, C., 2013. Levantine Intermediate Water characteristics: an astounding general misunderstanding! Sci. Mar. 77 (2), 217−232.

Napolitano, E., Iacono, R., Ciuffardi, T., Reseghetti, F., Poulain, P.-M., Notarstefano, G., 2019. The Tyrrhenian intermediate water (TIW): characterization and formation mechanisms. Prog. Oceanogr. 170, 53−68.

Nittis, K., Lascaratos, A., Theocharis, A., 2003. Dense water formation in the Aegean Sea: numerical simulations during the eastern Mediterranean transient. J. Geophys. Res. 108 (C9), 8120.

Orlić, M., Gacic, M., La Violette, P., 1992. The currents and circulation of the Adriatic Sea. Oceanol. Acta 15 (2), 109−124.

Ovchinnikov, I.M., 1984. the formation of intermediate water in the Mediterranean Sea. Oceanology 24, 168−173.

Ozer, T., Gertman, I., Gildor, H., Goldman, R., Herut, B., 2020. Evidence for recent thermohaline variability and processes in the deep water of the Southeastern Levantine Basin, Mediterranean Sea. Deep-Sea Res. Part II 171, 104651.

Özsoy, E., Hecht, A., Ünlüata, Ü., Brenner, S., Sur, H.I., Bishop, J., Latif, M.A., Rozentraub, Z., Oğuz, T., 1993. A synthesis of the Levantine Basin circulation and hydrography, 1985−1990. Deep Sea Res. Part II Top. Stud. Oceanogr. 40 (6), 1075−1119.

Pinardi, N., Navarra, A., 1993. Baroclinic wind adjustment processes in the Mediterranean Sea. Deep Sea Res II 40 (6), 1299−1326.

Pinardi, N., Korres, G., Lascaratos, A., Roussenov, V., Stanev, E., 1997. Numerical simulation of the interannual variability of the Mediterranean Sea upper ocean circulation. Geophys. Res. Lett. 24 (4), 425−428.

Pinardi, N., Zavatarelli, M., Adani, M., Coppini, G., Fratianni, C., Oddo, P., Simoncelli, S., Tonani, M., Lyubartsev, V., Dobricic, S., Bonaduce, A., 2015. Mediterranean Sea large-scale low-frequency ocean variability and water mass formation rates from 1987 to 2007: a retrospective analysis. Prog. Oceanogr. 132, 318−332.

Pinardi, N., Cessi, P., Borile, F., Wolfe, C.L., 2019. The Mediterranean Sea overturning circulation. J. Phys. Oceanogr. 49 (7), 1699−1721.

Pinot, J.-M., Ganachaud, A., 1999. The role of winter intermediate waters in the spring-summer circulation of the Balearic Sea: 1. Hydrography and inverse box modelling. J. Geophys. Res. 104 (C12), 29843−29864.

Pisacane, G., Artale, V., Calmanti, S., Rupolo, V., 2006. Decadal oscillations in the Mediterranean Sea: a result of the overturning circulation variability in the eastern basin? Clim. Res. 31 (2−3), 257−271.

Pollak, M.I., 1951. The sources of the deep water in the eastern Mediterranean. J. Mar. Res. 10 (1), 128−152.

Robinson, A.R., Malanotte-Rizzoli, P., Hecht, A., Michelato, A., Roether, W., Theocharis, A., Ünlüata, U., Pinardi, N., Artegiani, A., Bergamasco, A., Bishop, J., Brenner, S.,

Christianidis, S., Gacic, M., Georgopoulos, D., Golnaraghi, M., Hausmann, M., Junghaus, H.-G., Lascaratos, A., Latif, M.A., Leslie, W.G., Lozano, C.J., Oguz, T., Özsoy, E., Papageorgiou, E., Paschini, E., Rozentroub, Z., Sansone, E., Scarazzato, P., Schlitzer, R., Spezie, G.-C., Tziperman, E., Zodiatis, G., Athanassiadou, L., Gerges, M., Osman, M., 1992. General circulation of the eastern Mediterranean. Earth Sci. Rev. 32 (4), 285−309.

Roether, W., Schlitzer, R., 1991. Eastern Mediterranean deep water renewal on the basis of chlorofluoromethane and tritium data. Dynam. Atmos. Oceans 15 (3−5), 333−354.

Roether, W., Manca, B.B., Klein, B., Bregant, D., Georgopoulos, D., Beitzel, V., Kovačević, V., Luchetta, A., 1996. Recent changes in eastern Mediterranean deep waters. Science 271 (5247), 333−335.

Roether, W., Klein, B., Manca, B.B., Theocharis, A., Kioroglou, S., 2007. Transient Eastern Mediterranean deep waters in response to the massive dense-water output of the Aegean Sea in the 1990s. Prog. Oceanogr. 74, 540−571.

Rousselet, L., Cessi, P., Forget, G., 2021. Coupling of the mid-depth and abyssal components of the global overturning circulation according to a state estimate. Sci. Adv. 7 (21) eabf5478.

Rubino, A., Hainbucher, D., 2007. A large abrupt change in the abyssal water masses of the eastern Mediterranean, Geophys. Res. Lett. 34, L23607.

Sankey, T., 1973. The formation of deep water in the northwestern Mediterranean. Prog. Oceanogr. 6, 159−179.

Schlitzer, R., Roether, W., Oster, H., Junghans, H.-G., Hausmann, M., Johannsen, H., Michelato, A., 1991. Chlorofluoromethane and oxygen in the eastern Mediterranean. Deep-Sea Res. 38 (12), 1531−1551.

Schott, F., Leaman, K.D., 1991. Observations with moored acoustic Doppler current profilers in the convection regime in the Golfe du Lion. J. Phys. Oceanogr. 21 (4), 558−574.

Schott, F., Visbeck, M., Send, U., 1994. open ocean deep convection, Mediterranean and Greenland seas. In: Malanotte-Rizzoli, P., Robinson, A.R. (Eds.), Ocean Processes in Climate Dynamics: Global and Mediterranean Examples, NATO ASI Series (Series C: Mathematical and Physical Sciences), vol. 419. Springer, Dordrecht.

Schroeder, K., Josey, S.A., Herrmann, M., Grignon, L., Gasparini, G.P., Bryden, H.L., 2010. Abrupt warming and salting of the western Mediterranean deep water after 2005: atmospheric forcings and lateral advection. J. Geophys. Res. 115, C08029.

Send, U., Testor, P., 2017. Direct observations reveal the deep circulation of the western Mediterranean Sea. J. Geophys. Res. Oceans 122, 10091−10098.

Send, U., Marshall, J., 1995. Integral effects of deep convection. J. Phys. Oceanogr. 25, 855−872.

Seyfried, L., Estournel, C., Marsaleix, P., Richard, E., 2019. Dynamics of the North Balearic Front during an autumn tramontane and mistral storm: air−sea coupling processes and stratification budget diagnostic. Ocean Sci. 15, 179−198.

Shapiro, G.I., Huthnance, J.M., Ivanov, V.V., 2003. Dense water cascading off the continental shelf. J. Geophys. Res. 108, 3390.

Simoncelli, S., Fratianni, C., Pinardi, N., Grandi, A., Drudi, M., Oddo, P., Dobricic, S., 2017. Mediterranean Sea Physical Reanalysis (MEDREA 1987-2015). Copernicus Monitoring Environment Marine Service. https://doi.org/10.25423/medsea_reanalysis_phys_006_004.

Simoncelli, S., Pinardi, N., Fratianni, C., Dubois, C., Notarstefano, G., 2018. Water mass formation processes in the Mediterranean sea over the past 30 years. In: Copernicus Marine

Service Ocean State Report, Issue 2, Copernicus Marine Service Ocean State Report, Journal of Operational Oceanography, vol. 11, pp. S1−S142. Suppl. 1.

Somot, S., Houpert, L., Sevault, F., Testor, P., Bosse, A., Taupier-Letage, I., Bouin, M.N., Waldman, R., Cassou, C., Sanchez-Gomez, E., Durrieu de Madron, X., Adloff, F., Nabat, P., Herrmann, M., 2018. Characterizing, modelling and understanding the climate variability of the deep water formation in the North-Western Mediterranean Sea. Clim. Dynam. 51, 1179−1210.

Spall, M.A., 2003. On the thermohaline circulation in flat bottom marginal seas. J. Mar. Res. 61, 1−25.

Spall, M.A., 2004. Boundary currents and water mass transformation in marginal seas. J. Phys. Oceanogr. 34, 1197−1213.

Speer, K., Tziperman, E., 1992. Rates of water Mass Formation in the north Atlantic ocean. J. Phys. Oceanogr. 22 (1), 93−104.

Stommel, H., Voorhis, A., Webb, D., 1971. Submarine Clouds in the Deep Ocean: surface cooling during late winter in the northwestern Mediterranean Sea causes large masses of water to sink to great depths. Am. Sci. 59 (6), 716−722.

Straneo, F., Kawase, M., 1999. Comparisons of localized convection due to a Localized forcing and to preconditioning. J. Phys. Oceanogr. 29, 55−68.

Straneo, F., 2006. Heat and freshwater transport through the central Labrador sea. J. Phys. Oceanogr. 36 (4), 606−628.

Supić, N., Vilibić, I., 2006. Dense water characteristics in the northern Adriatic in the 1967−2000 interval with respect to surface fluxes and Po river discharge rates. Estuar. Coast Shelf Sci. 66 (3−4), 580−593.

Sur, H.I., Ozsoy, E., Umluata, U., 1992. Simultaneous deep and intermediate depth convection in the Northern Levantine Sea, winter 1992. Oceanol. Acta 16 (1), 33−43.

Swallow, J.C., Caston, G.F., 1973. The preconditioning phase of MEDOC 1969. Part I. Observations. Deep-Sea Res. 20, 429−448.

Talley, L.D., 2013. Closure of the global overturning circulation through the Indian, Pacific, and southern oceans: schematics and transports. Oceanography 26 (1), 80−97.

Tchernia, P., 1960. Hydrologic d'hiver en Méditerranée occidentale. Cah. Oceanogr. 12 (3), 184−198.

Testor, P., Bosse, A., Houpert, L., Margirier, F., Mortier, L., Legoff, H., Dausse, D., Labaste, M., Karstensen, J., Hayes, D., Olita, A., Ribotti, A., Schroeder, K., Chiggiato, J., Onken, R., Heslop, E., Mourre, B., D'ortenzio, F., Mayot, N., Lavigne, H., de Fommervault, O., Coppola, L., Prieur, L., Taillandier, V., Durrieu de Madron, X., Bourrin, F., Many, G., Damien, P., Estournel, C., Marsaleix, P., Taupier-Letage, I., Raimbault, P., Waldman, R., Bouin, M.N., Giordani, H., Caniaux, G., Somot, S., Ducrocq, V., Conan, P., 2018. Multiscale observations of deep convection in the northwestern Mediterranean Sea during winter 2012−2013 using multiple platforms. J. Geophys. Res. Oceans 123, 1745−1776.

Theocharis, A., Balopoulos, E., Kioroglou, S., Kontoyiannis, H., Iona, A., 1999. A synthesis of the circulation and hydrography of the south Aegean Sea and the Straits of the Cretan Arc (March 1994−January 1995). Prog. Oceanogr. 44 (4), 469−509.

Theocharis, A., Krokos, G., Velaoras, D., Korres, G., 2014. An internal mechanism driving the alternation of the eastern Mediterranean dense/deep water sources. In: Borzelli, G.L.E., Gačić, M., Lionello, P., Malanotte-Rizzoli, P. (Eds.), The Mediterranean Sea. https://doi.org/10.1002/9781118847572.ch8.

Toggweiler, J.R., Samuels, B., 1993. Is the magnitude of the deep outflow from the Atlantic Ocean actually governed by Southern Hemisphere winds?. In: The Global Carbon Cycle. Springer, Berlin, Heidelberg, pp. 303–331.

Tsimplis, M.N., Zervakis, V., Josey, S.A., Peneva, E.L., Struglia, M.V., Stanev, E.V., Theocharis, A., Lionello, P., Malanotte-Rizzoli, P., Artale, V., Tragou, E., 2006. Changes in the oceanography of the Mediterranean Sea and their link to climate variability. In: Developments in Earth and Environmental Sciences, vol. 4. Elsevier, pp. 227–282.

Turchetto, M., Boldrin, A., Langone, L., Miserocchi, S., Tesi, T., Foglini, F., 2007. Particle transport associated with the Bari canyon (southern Adriatic Sea). Mar. Geol. 246, 231–247.

Ulses, C., Estournel, C., Puig, P., Durrieu de Madron, X., Marsaleix, P., 2008. Dense water cascading in the northwestern Mediterranean during the cold winter 2005. Quantification of the export through the Gulf of Lion and the Catalan margin. Geophys. Res. Lett. 35, L07610.

Velaoras, D., Krokos, G., Nittis, K., Theocharis, A., 2014. Dense intermediate water outflow from the Cretan Sea: a salinity driven, recurrent phenomenon, connected to thermohaline circulation changes. J. Geophys. Res. Oceans 119 (8), 4797–4820.

Velaoras, D., Zervakis, V., Theocharis, A., 2021. The physical characteristics and dynamics of the Aegean water masses. In: The Handbook of Environmental Chemistry. Springer, Berlin, Heidelberg.

Verri, G., Pinardi, N., Oddo, P., Ciliberti, S.A., Coppini, G., 2018. River runoff influences on the Central Mediterranean overturning circulation. Clim. Dynam. 50, 1675–1703.

Vigo, M.I., Garcia, D., Chao, B.F., 2005. Change of sea level trend in the Mediterranean and Black seas. J. Mar. Res. 63, 1085–1100.

Vilibic, I., 2003. An analysis of dense water production on the North Adriatic shelf. Estuar. Coast Shelf Sci. 56, 861–867.

Vilibić, T., Supić, N., 2005. Dense water generation on a shelf: the case of the Adriatic Sea. Ocean Dynam. 55 (5–6), 403–415.

Waldman, R., Somot, S., Herrmann, M., Testor, P., Estournel, C., Sevault, F., Prieur, L., Mortier, L., Coppola, L., Taillandier, V., Conan, P., Dausse, D., 2016. Estimating dense water volume and its evolution for the year 2012–2013 in the north-western Mediterranean Sea: an observing system simulation experiment approach. J. Geophys. Res. Oceans 121, 6696–6716.

Waldman, R., Somot, S., Herrmann, M., Bosse, A., Caniaux, G., Estournel, C., Houpert, L., Prieur, L., Sevault, F., Testor, P., 2017. Modeling the intense 2012–2013 dense water formation event in the northwestern Mediterranean Sea: evaluation with an ensemble simulation approach. J. Geophys. Res. Oceans 122, 1297–1324.

Waldman, R., Brüggemann, N., Bosse, A., Spall, M., Somot, S., Sevault, F., 2018. Overturning the Mediterranean thermohaline circulation. Geophys. Res. Lett. 45, 8407–8415.

Wang, X.H., Oddo, P., Pinardi, N., 2006. On the bottom density plume on coastal zone off Gargano (Italy) in the southern Adriatic Sea and its interannual variability. J. Geophys. Res. 111, C03S17.

Wolfe, C.L., Cessi, P., 2011. The adiabatic Pole-to-Pole overturning circulation. J. Phys. Oceanogr. 41 (9), 1795–1810. https://doi.org/10.1175/2011JPO4570.1.

Wu, P., Haines, K., 1996. Modeling the dispersal of Levantine Intermediate Water and its role in Mediterranean deep water formation. J. Geophys. Res. 101 (C3), 6591–6660.

Wu, P., Haines, K., Pinardi, N., 2000. Toward an understanding of deep-water renewal in the eastern Mediterranean. J. Phys. Oceanogr. 30, 443–458.

Wüst, G., 1961. On the vertical circulation of the Mediterranean Sea. J. Geophys. Res. 66, 3261−3271.

Young, W.R., 2012. An exact thickness-weighted average formulation of the Boussinesq equations. J. Phys. Oceanogr. 42 (5), 692−707.

Zavatarelli, M., Mellor, G.L., 1995. A numerical study of the Mediterranean Sea circulation. J. Phys. Oceanogr. 25 (6), 1384−1414.

Zervakis, V., Georgopoulos, D., Drakopoulos, P.G., 2000. The role of the North Aegean in triggering the recent Eastern Mediterranean climatic changes. J. Geophys. Res. 105 (C11), 103−116.

Zore-Armanda, M., 1963. Mixing of three water types in the south Adriatic. Rapp. Proces Verbaux Reunions Comm. Int. pour Explor. Sci. Mer Mediterr. 17 (3), 879−885.